Published in final edited form as:
J Am Chem Soc. 2010 March 10; 132(9): 3164–3176. doi:10.1021/ja909996p.

Comparative Analysis of Small Molecules and Histone Substrate Analogs as LSD1 Lysine Demethylase Inhibitors

Jeffrey C. Culhane[a], **Dongqing Wang**[b], **Paul M. Yen**[b,c], and **Philip A. Cole**[a,*]

[a]Dept. of Pharmacology and Molecular Sciences, Johns Hopkins University School of Medicine, Baltimore, MD 21205

[b]Dept. of Medicine, Johns Hopkins Bayview Medical Center, Baltimore, MD 21224

[c]Cardiovascular and Metabolic Diseases Program, Duke-NUS Graduate Medical School, Singapore, 169857

Abstract

LSD1 is a flavin dependent histone demethylase that oxidatively removes methyl groups from Lys-4 of histone H3. LSD1 belongs to the amine oxidase enzyme superfamily which utilize molecular oxygen to transform amines to imines that are hydrolytically cleaved to formaldehyde. In prior studies, it has been shown that monoamine oxidase inhibitory scaffolds such as propargylamines and cyclopropylamines can serve as mechanism-based inactivators of LSD1. Propargylamine-histone H3 peptide analogs are potent LSD1 inhibitors whereas small molecule antidepressant MAO acetylenic inhibitors like pargyline do not inhibit LSD1. In contrast, the small molecule MAO cyclopropylamine inhibitor tranylcypromine is a time-dependent LSD1 inhibitor but *exo*-cyclopropylamine-peptide substrate analog is not. To provide further insight into small molecule versus peptide relationships in LSD1 inhibition, herein we further our analysis of warheads in peptide scaffolds to include the chlorovinyl, *endo*-cyclopropylamine, and hydrazine-functionalities as LSD1 inactivators. We find that chlorovinyl-H3 is a mechanism-based LSD1 inactivator whereas *endo*-cyclopropylamine-H3 does not show time-dependent inactivation. The hydrazine-H3 was shown to be the most potent LSD1 suicide inhibitor yet reported, more than 20-fold more efficient in inhibiting demethylation than propargylamine-H3 derivatives. We re-explored MAO antidepressant agent phenelzine (phenethylhydrazine), previously reported to be a weak LSD1 inhibitor, and found that it is far more potent than previously appreciated. We show that phenelzine can block histone H3K4Me demethylation in cells, validating it as a pharmacologic tool and potential lead structure for anti-cancer therapy.

Post-translational modification (PTM) of histones on lysines regulates gene expression by remodeling chromatin and is a central focus of epigenetic studies.[1,2] Among the many PTMs that reversibly modify chromatin, lysine methylation provides for a rich array of biological readouts.[3,4] For example, methylation of Lys-4 of histone H3 is a mark of gene activation, whereas Lys-9 methylation is more often associated with gene silencing. The relatively recent discovery of histone lysine demethylases has helped round out our understanding of the factors that control methyl-Lys stability.[5,6] Included among the histone demethylases are the flavin dependent enzymes LSD1 and LSD2 and the iron-dependent Jmj catalysts.[5–7]

LSD1 is a member of the amine oxidase superfamily and utilizes a non-covalently bound FAD cofactor in the oxidative removal of methyl groups, specifically from Lys-4 of histone H3.[5,8] The catalytic cycle of methyl removal produces a molecule each of formaldehyde and

*To whom correspondence should be addressed. pcole@jhmi.edu. Telephone: (410) 614-8849. Fax: (410) 955-3023.

H_2O_2 while consuming O_2 (Scheme 1).[5,8] Dictated by the inherent limitations of the flavin chemistry, LSD1 can only function in the removal of the mono- and dimethyl- species of Lys-4.[5] LSD1 functions as a transcriptional repressor and is a component of various transcriptional co-repressor complexes that often include HDAC1/2 and CoREST.[9–12] In addition to processing histone proteins, LSD1 can demethylate H3-tail peptides, requiring at least 15 amino acid residues for efficient demethylation.[5,13] Inhibitors of LSD1 would be expected, in general, to reactivate gene expression of silenced genes, which might have utility in the treatment of cancer and other diseases.[14,15] Such compounds could for example be synergistic with HDAC inhibitors.[14,15]

The flavin-dependent amine oxidase family of enzymes has been intensively studied over the past 50 years as clinical targets for human diseases.[16] In particular, the monoamine oxidases, MAO-A and MAO-B, play key roles in the clearance of neurotransmitters.[16–18] Selective MAO-A/B suicide inactivators have enjoyed decades of clinical success in the treatment of major depression and neurodegenerative disorders such as Parkinson's disease.[16–18] Since LSD1 and MAO-A/B share a common mechanism for the oxidative cleavage of the unactivated nitrogen-carbon bonds of their substrates, many of the known MAO inactivators have been tested as LSD1 inhibitors.[14] Tranylcypromine, a cyclopropylamine containing small molecule, has been characterized as an LSD1 inactivator through biochemical, spectroscopic, and crystallographic procedures.[14,19,20] The hydrazine-containing MAO inhibitor and antidepressant phenelzine has also been reported to be a weak LSD1 inhibitor.[14] On the other hand, pargyline, a propargylamine containing small molecule initially suggested to be an LSD1 inhibitor, has failed in subsequent studies to appreciably inactivate LSD1.[13,14]

Interestingly, the propargylamine functionality in the context of a histone H3-21 peptide (**1**) has yielded potent time- and concentration-dependent inactivation of LSD1 (Figure 1).[21–23] Characterization of the inactivation by **1** and its *N*-methyl analog **2** by kinetic, spectroscopic, and crystallographic studies have revealed key mechanistic and structural information about the nature of inactivation and substrate recognition.[21–23] In particular, an X-ray crystal structure of LSD1 inactivated by **2** has provided a model for histone H3 substrate recognition.[23] These studies have established that MAO inhibitor functionalities can target LSD1 but leave open the range of warheads and the contextual relationship to substrate analogs that can inhibit this enzyme. In this study, we investigate other known MAO-A/B inactivator motifs for incorporation into histone H3-21 peptides in the search for increasingly potent inactivators of LSD1. We compare and contrast the behavior of small molecules versus peptide analogs containing inhibitory warheads. Importantly, we identify the hydrazine motif as the most potent LSD1 inhibitor functionality in the context of peptides and small molecules.

Results and Discussion

Chlorovinyl-H3 peptide analog synthesis and LSD1 inhibition

The 3-chloroallylamine functionality has the ability to inactivate flavin-dependent amine oxidases,[24,25] and we therefore sought to generate H3-chlorovinyl analogs **3** and **4**. For this purpose, we prepared *cis*-3-chloroallylamine hydrochloride from commercially available *cis*-1,3-dichloropropene utilizing the Gabriel synthetic approach.[25] The corresponding *trans*-3-chloroallylamine hydrochloride was generated in a similar fashion from commercially available *rac*-1,3-dichloropropene followed by selective precipitation.[25] Peptide analogs **3** and **4** were synthesized utilizing our previously reported strategy.[21] Briefly, a 21 amino acid *N*-terminal histone H3 tail peptide was constructed on solid support incorporating an oxa-analog of lysine, 6-hydroxynorleucine,[21] at the fourth position. Following mesylation of the alcohol, the peptide was cleaved from the resin and universally deprotected, allowing for reverse phase high performance liquid chromatography (RP-HPLC) purification of the mesylate peptide

(**5**). Displacement of the mesylate with small molecule amines afforded the desired peptides in 40–50% yield (Scheme 2).

Peptides **3** and **4** were assayed against recombinant GST-LSD1 utilizing a horseradish peroxidase coupled assay for the detection of H_2O_2 produced in the demethylase catalytic cycle.[21] *cis*-3-chloroallyl-Lys-4 H3-21 (**3**) and *trans*-3-chloroallyl-Lys-4 H3-21 (**4**) both displayed time- and concentration-dependent inactivation of LSD1 with $K_{i(inact)} = 0.955 \pm 0.15$ μM and 0.763 ± 0.12 μM, and $k_{inact} = 0.545 \pm 0.038$ min^{-1} and 0.128 ± 0.0087 min^{-1}, respectively (Figure 2, Table 1). It has been hypothesized that the chlorovinyl mechanism of inactivation of MAO is similar to that of a propargylamine inactivator.[24] We propose, in analogy to previous studies on MAOs, that oxidation of **3** and **4** produces α,β-unsaturated iminium electrophiles that are capable of Michael addition with a nearby nucleophile. The presence of the chloride as a leaving group allows for the generation of a conjugated diamine linker (Scheme 3). The four-fold difference in the inactivation rate constants for the *cis* (**3**) versus *trans* (**4**) isomer may be related to altered oxidation rates or follow-on nucleophilic attack differences that stem from the steric and spatial orientation of the chloride atom in the active site of the enzyme. The efficiency of inactivation ($k_{inact}/K_{i(inact)}$) of LSD1 by **3** is similar to that of the propargylamine compound **1** and within 5-fold of the $k_{inact}/K_{i(inact)}$ of the more potent *N*-methylpropargylamine peptide **2** (Figure 1, Table 1).

To further investigate the inactivation processes for **3** and **4**, we employed UV-visible spectroscopy to characterize possible flavin adducts, as seen previously with compounds **1** and **2**.[21–23] LSD1-bound FAD has two characteristic absorption maxima in the 350–550 nm range, attributed to the fully oxidized flavin and the one electron reduced semiquinone form.[26] As with **1**, treatment of LSD1 with inactivator **3** or **4** leads to the near bleaching of the flavin spectrum. The *cis* isomer (**3**) results in a newly formed maximum at 383 nm, while the *trans* isomer (**4**) induces a new maximum at a wavelength less than 350 nm (Figure 3). It is possible that these spectroscopic shifts correspond to inhibitor-flavin adducts with different stereochemistry.

The FAD molecule of LSD1 is non-covalently bound. Inactivator-FAD adducts can therefore be isolated from the protein prior to analysis by MALDI-TOF mass spectrometry.[20–23] Mass spec analysis of denatured **3** or **4**-inactivated LSD1 showed peaks at *m/z* = 3077, corresponding to the mass of the peptide and the FAD following the loss of the chloride atom, as proposed in Scheme 3 (Figure 4). Additionally, for both inactivation reactions, a peak corresponding to H3-21 peptide is noted at *m/z* = 2255, this degradation product may be generated from an active site water molecule attacking the oxidatively activated iminum species at the alpha carbon as shown in Scheme 3, path b. Another potential degradation peak is also noted at *m/z* = 2290. The mass of the product corresponds to the loss of HCl from the oxidized intermediates produced from **3** or **4**. It is formally possible that after the activation of **3** and **4** by LSD1 an intramolecular cyclization of the peptide thru Michael addition, potentially within or outside the active site, leads to the degradation of the inactivator, as shown in Scheme 3, path c. Consistent with these degradation mechanisms of the inactivator, only a minor peak in the mass spectrum corresponding to the mass of peptide **3** or **4**, **is observed after LSD1 treatment**. Taken together, these studies support an inactivation mechanism involving flavin attack on the conjugated imine as proposed in Scheme 3. It is difficult to obtain precise partition ratios, however, because of the challenge in separating and quantifying the various enzymatic products by HPLC.

Endo-Cyclopropyl-H3 synthesis and LSD1 inhibition analysis

The small molecule tranylcypromine displays moderately potent time- and concentration-dependent inactivation of LSD1 (Table 1).[20] In contrast, an H3-21 peptide that incorporated an *exo*-cyclopropyl-Lys-4 functionality (**6**) was found to be a reversible inhibitor (estimated

K_i = 2.70 ± 0.74 μM), but did not inactivate LSD1 (Figure 1, Table 1).[22] It can be rationalized that this result is due to steric clashes related to the bulky *exo*-cyclopropyl group of **6**. To explore this further, we synthesized the corresponding *endo*-cyclopropylamine containing peptides **7** and **8** which better mimic the structural arrangements found in tranylcypromine (Figure 1). To that end, an efficient synthesis of the Fmoc-*endo*-cyclopropyl-Lys(Boc)-OH (**9**) and Fmoc-*endo*-dimethylcyclopropyl-Lys-OH (**10**) monomers was designed for their direct incorporation during solid phase peptide synthesis. While previous syntheses exist for *endo*-cyclopropyl containing lysine residues,[27] our route maintains the proper four carbon chain between the peptide backbone and the epsilon nitrogen of lysine.

Perbenzylation of commercially available L-Glu (**11**), selective reduction of the side chain ester to the alcohol (**12**), and Swern oxidation yields the amino aldehyde **13** in an overall 43% yield (Scheme 4).[28] Horner-Wadsworth-Emmons reaction of the aldehyde **13** with *t*-butyl diethylphosphonoacetate provides the α, β-unsaturated ester **14**[29] for cyclopropanation with diazomethane yielding **15**.[30] The α, β-cyclopropyl *t*-butyl ester **15** can be selectively hydrolyzed under acidic conditions allowing the acid **16** to undergo Curtius rearrangement to yield the *tert*-butyl carbamate protected cyclopropylamine **17**.[31] Removal of the benzyl esters can be accomplished under hydrogenation conditions in a Parr shaker to provide the deprotected α-amino acid. Treatment with Fmoc-OSu yields Fmoc-*endo*-cyclopropyl-Lys (Boc)-OH (**9**). TFA treatment of **9** allows for the incorporation of two methyl groups by reductive amination, yielding Fmoc-*endo*-dimethylcyclopropyl-Lys-OH (**10**) (Scheme 5).[32] Fmoc amino acids **9** and **10** were used in standard Fmoc SPPS to provide peptides **7** and **8**.[22]

In contrast to the results with propargylamine and chlorovinyl derivatives, *endo*-cyclopropylamine containing peptides **7** and **8** failed to inactivate LSD1. Both peptides displayed a reversible mode of inhibition with an estimated K_i = 6.11 ± 0.86 μM and 24.2 ± 2.7 μM, respectively, determined by Dixon analysis assuming a competitive inhibitory model (Figure 5). Interestingly, the dimethylated peptide (**8**) displayed lower potency than the unmethylated analog (**7**), although **8** was projected to be the better model of the dimethyl-Lys-4 substrate. This result suggests that the incorporation of the cyclopropyl moiety not only as *exo* as in peptide **6**,[22] but also as *endo* effects the binding of the inhibitor peptide enough to eliminate oxidative turnover by LSD1. We suggest that the radical/cation stabilizing function of the benzyl group, lacking in **7** and **8**, plays a key effector function in the tranylcypromine inactivation mechanism of LSD1.

Hydazino analogs as LSD1 inhibitors

As mentioned, phenelzine was previously shown to be a weak inhibitor of LSD1, suggested to be 20-fold weaker than tranylcypromine.[14] To analyze this further, we embarked on the synthesis of hydrazine analog **18**. This was readily achieved by displacement of the mesylate functionality with hydrazine akin to generation of inactivators **3** and **4** (Scheme 2).[21] Initial enzymatic inhibition studies revealed compound **18** to be a highly potent time-dependent inhibitor of LSD1. Limited sensitivity of the 4-aminoantipyrine and 3,5-dichloro-2-hydroxybenzenesulfonic acid coupled assay[21] prevented a precise determination of the inhibitory parameters. We therefore utilized a more sensitive Amplex® Red[33] coupled assay for the detection of H_2O_2 produced during enzymatic turnover of substrate. We determined that hydrazine analog **18** had a $K_{i(inact)}$ and $k_{(inact)}$ of 4.35 ± 0.86 nM and 0.247 ± 0.018 min^{-1}, respectively (Figure 6). This makes hydrazino-Lys-4 H3-21 (**18**) approximately 25-fold more potent than **2**, the previous best in class LSD1 inactivator which contains the *N*-methylpropargylamine motif (Table 1). The significantly lower $K_{i(inact)}$ of **18** compared with that of **1** and **2** was unexpected and may reflect a higher affinity for the encounter complex between **18** and LSD1. If so, this may suggest that the lower pK_a of the hydrazine versus the amino functionality contributes to enhanced affinity, and that the neutral rather than the

positively charged species preferentially binds to LSD1. Alternatively, the $K_{i(inact)}$ of **18** may not correspond to its K_d but instead may be composed of a series of complex rate constants.

Spectroscopic analysis of **18** inactivated LSD1 showed loss of the visible maxima, consistent with flavin modification (Figure 7A). The MALDI mass spectrum of the inactivated mixture revealed a peak with *m/z* =3024, consistent with the formation of a peptide-FAD adduct with concurrent loss of N_2 (Figure 7B). In accordance with prior proposals for phenelzine inactivation of MAO, we suggest an LSD1 inactivation mechanism that initially involves a two electron oxidation to form the corresponding diazene (Scheme 6, path a). We propose that after re-oxidation of the FAD by molecular oxygen, a two electron oxidation of the diazene yields the diazonium species, an excellent leaving group. Attack from the N^5 of the reduced flavin leads to the inactivator-FAD adduct with lose of N_2 (Scheme 6 path b).[34,35] Interestingly, the mass spectrum also shows evidence of two peptide degradation pathways. The first correlates to an aldehyde containing peptide at *m/z* = 2253. This product could potentially stem from non-enzymatic hydrolysis of a hydrazone that can be produced during the initial oxidation of the inhibitor to the diazene (Scheme 6, path d). A second degradation correlates to the loss of N_2H_2 from the oxidatively activated diazene peptide (*m/z* = 2237). This could potentially be produced through the abstraction of the beta proton and lose of N_2 yielding an olefin (Scheme 6, path c), or through an internal cyclization of the peptide as similarly proposed previously in the case of the chlorovinyl inactivators (Scheme 3). Quantification of the relative product ratios in the LSD1 reaction with **18** is difficult because of the challenge of separating and detecting these chemical species by HPLC. We cannot also not rule out the possibility that the LSD1 inactivation mechanism related to **18** also involves some covalent enzyme modification reactions.

The impressive inhibitory characteristics with hydrazino-Lys-4 H3-21 (**18**) led us to re-investigate the inhibitory characteristics of phenelzine for LSD1. Remarkably, we found that phenelzine showed a $K_{i(inact)}$ of 17.6 ± 2.8 μM and a $k_{(inact)}$ of 0.955 ± 0.085 min^{-1} (Figure 8). To rule out that the perceived LSD1 inhibition was somehow related to the interfering action of phenelzine on peroxide detection, we performed the following additional experiments. We demonstrated that inactivation of LSD1 was greater when pre-treated with phenelzine, in the absence of horseradish peroxidase, followed by assay (Figure 9A). We showed that additional horseradish peroxidase failed to relieve the LSD1 inhibition (Figure 9B). Finally, we determined in a direct assay using mass spectrometry that phenelzine-treated LSD1 was unable to induce loss of a methyl group from an H3-21 dimethyl-Lys substrate peptide (Figure 10). While considerably less potent than hydrazino-Lys-4 H3-21 (**18**), phenelzine is approximately 35-fold more efficient as an LSD1 inactivator than tranylcypromine in our hands, and appears to be comparable to a newly described class of tranylcypromine analogs.[36] The inactivation efficiency of phenelzine toward LSD1 appears comparable to, if not greater than, its inhibitory effect versus MAOs.[37] Although we cannot account for the inhibitory differences regarding tranylcypromine and phenelzine between our work and a prior study,[14] we note that the assay methods were quite distinct. Moreover, the tranylcypromine LSD1 inhibition parameters measured previously by us[20] were in close agreement with those of Schmidt and McCafferty.[19]

Given the relative in vitro inhibitory potency of phenelzine toward recombinant LSD1, we considered that phenelzine might also block LSD1 in live cells. To examine the effects of phenelzine as a demethylase inhibitor in cells, we explored the effects of phenelzine on a thyroid hormone (T3) inhibited TSHalpha luciferase reporter transfected in cells.[38] As shown, LSD1 inhibition increases luciferase activity both in the absence and presence of T3 but maintains negative regulation by T3 (Figure 11). Assessment of the methylation status of Lys-4 of histone H3 by ChIP (chromatin immunoprecipation) in response to phenelzine, revealed that mono and dimethylation of the TSHalpha reporter region was enhanced by phenelzine, whereas

the trimethylation level was unaffected (Figure 12). These findings suggest that mono- and dimethylation of Lys-4 H3 may enhance basal transcription of TSHalpha promoter in the absence or presence of T3. These results correlate with that expected for LSD1 inhibition (as opposed to a trimethyl-Lys demethylase) and establish the pharmacologic value of phenelzine as an epigenetic probe.

Summary

In this study we have designed, synthesized, and examined several novel H3 tail peptide analogs containing classical monoamine oxidase warhead groups as LSD1 inhibitors. The chlorovinyl-containing inhibitors are comparable in potency to alkynyl inhibitors described previously, whereas the hydrazine containing H3 peptide is the most potent suicide inactivator known for LSD1. Consistent with this finding, the hydrazine containing MAO inhibitor phenelzine is the most potent small molecule LSD1 inhibitor that has emerged from our studies. Its potency is such that the pharmacology of phenelzine, which is clearly active against MAOs, is likely enhancing Lys-4 H3 methylation in its therapeutically useful range. It could for example synergize with HDAC and DNA methyltransferase inhibitors to induce the re-expression of silenced tumor suppressor genes.[39,40]

In contrast to the peptide and small molecule hydrazines, there is discordance in inactivation potential of propargyl and cyclopropyl inhibitors of LSD1. Whereas propargylamine peptide inhibitors are efficient LSD1 inhibitors, peptide cyclopropyl compounds are not. This contrasts with the pargyline and tranylcypromine effects on LSD1. Taken together, these studies reveal a complex mosaic in molecular recognition among LSD1, its substrates, and inhibitory compounds.

Experimental

General

All synthetic reactions were carried out under an inert argon atmosphere using standard techniques. Solvents were purchased from Aldrich as anhydrous and used as is. NMR spectra were recorded on a Varian 400 MHz spectrometer. MALDI-TOF spectra were recorded on a Applied Biosystems Voyager DE-STR mass spectrometer. ESI-TOF spectra were recorded on an Applied Biosystems Sciex instrument.

***cis*-3-chloroallyl-Lys-4 H3-21 (3)—**Lyophilized mesyl-Lys-4 H3-21 (**5**) (5.0 mg, 2.1 μmol) was dissolved in 500 μL of 1:1 H_2O:CH_3CN. *cis*-3-chloroallylamine hydrochloride (82 mg, 640 μmol) in 500 μL of 1:1 H_2O:CH_3CN was added to the solution followed by freshly distilled triethylamine (120 μL, 860 μmol). The reaction rotated 70 hours at 25 °C. The crude reaction mixture was diluted to 15 mL with H_2O, acidified to pH 2 with TFA, and lyophilized to an oil. The oil was diluted to 3 mL with H_2O and injected onto a prep scale column for RP-HPLC purification. Analysis by MALDI-TOF showed an expected/observed *m/z* = 2328.31.

***trans*-3-chloroallyl-Lys-4 H3-21 (4)—**Lyophilized mesyl-Lys-4 H3-21 (**5**)(5.0 mg, 2.1 μmol) was dissolved in 500 μL of 1:1 H_2O:CH_3CN. *trans*-3-chloroallylamine hydrochloride (82 mg, 640 μmol) in 500 μL of 1:1 H_2O:CH_3CN was added to the solution followed by freshly distilled triethylamine (120 μL, 860 μmol). The reaction rotated 70 hours at 25 °C. The crude reaction mixture was diluted to 25 mL with H_2O, acidified to pH 2 with TFA, and lyophilized to an oil. The oil was diluted to 3 mL with H_2O and injected onto a prep scale column for RP-HPLC purification. Analysis by MALDI-TOF showed an expected/observed *m/z* = 2328.31.

mesyl-Lys-4 H3-21 (5)—The primary alcohol of resin bound peptide was treated with 20 equivalents of mesyl chloride in the presence of 40 equivalents of triethylamine in

tetrahydrofuran for 20 hours at room temperature. Universal deprotection and cleavage of the peptide from the Wang resin, in the presence of the mesylate, was accomplished by treating the resin bound peptide with Reagent K (95:5 trifluoroacetic acid: H_2O in the presence of phenol, ethanedithiol, and thioanisole) for 4 hours at room temperature. Precipitation of the peptide with diethyl ether followed by lyophilization yielded crude peptide as an off-white solid that was purified by prep scale RP-HPLC. Analysis by MALDI-TOF showed an expected/observed *m/z* = 2333.28.

***endo*-cyclopropyl-Lys-4 H3-21 (7)—**Standard Fmoc solid phase peptide synthesis technique was utilized to assemble the *endo*-cyclopropyl-Lys-4 H3-21 peptide. The *endo*-cyclopropyl-Lys-4 residue was inserted as the Fmoc monomer **9**. Universal deprotection and cleavage of the peptide from the Wang resin was accomplished with Reagent K (95:5 trifluoroacetic acid: H_2O in the presence of phenol, ethanedithiol, and thioanisole) for 5 hours at 25 °C. Precipitation of the peptide with diethyl ether followed by lyophilization yielded crude peptide as an off-white solid that was purified by prep scale RP-HPLC. Analysis by MALDI-TOF showed an expected/observed *m/z* = 2266.31.

***endo*-dimethylcyclopropyl-Lys-4 H3-21 (8)—**Standard Fmoc solid phase peptide synthesis technique was utilized to assemble the *endo*-dimethylcyclopropyl-Lys-4 H3-21 peptide. The *endo*-dimethylcyclopropyl-Lys-4 residue was inserted as the Fmoc monomer **10**. Universal deprotection and cleavage of the peptide from the Wang resin was accomplished with Reagent K (95:5 trifluoroacetic acid: H_2O in the presence of phenol, ethanedithiol, and thioanisole) for 5 hours at 25 °C. Precipitation of the peptide with diethyl ether followed by lyophilization yielded crude peptide as an off-white solid that was purified by prep scale RP-HPLC. Analysis by MALDI-TOF showed an expected/observed *m/z* = 2294.35.

Fmoc-*endo*-cyclopropyl-Lys(Boc)-OH (9)—The benzylated amino acid **17** (600 mg, 1.1 mmol) in 10 mL of absolute ethanol had 100 mg of palladium on carbon (10 wt% wet) added to it and the suspension degassed with argon. Hydrogenation, using a Parr shaker apparatus, was performed for 15 hours under 55 psi of hydrogen gas. Following the hydrogenation, 10 mL of H_2O was added to the suspension to dissolve the free amino acid. The suspension was filtered through a plug of celite and washed with H_2O and ethanol. The solvent was removed *in vacuo* to yield a white solid which was then suspended in 10 mL of 1:1 H_2O: Acetone. Potassium carbonate (684 mg, 4.95 mmol) and Fmoc-succinimidyl carbonate (668 mg, 1.98 mmol) were added and the reaction was stirred at 25 °C for 15 hours. The reaction was concentrated *in vacuo* to an off-white solid and purified by RP-HPLC on a prep scale column using a H_2O: Acetonitrile gradient with 0.05% formic acid to yield 106 mg (20%) of **9** as a white powder following lyophilization. ^1H (CD_3Cl_3, 400 MHz): δ 7.75 (d, *J* = 7.2 Hz, 2H); 7.58 (d, *J* = 7.2 Hz, 1H); 7.38 (t, *J* = 7.2 Hz, 2H); 7.29 (t, *J* = 7.2 Hz, 2H); 5.67 (d, 1H); 4.95 (d, 1H); 4.67 (m, 1H); 4.37 (t, 2H); 4.21 (d, 1H); 2.46 (m, 1H); 2.20 (m, 1H); 2.06 (m, 1H); 1.79 (m, 2H); 0.94 (m, 1H); 0.62 (m, 1H); 0.48 (m, 1H). HRMS: expected: 481.23 [M+H], observed: 503.2125 [M+Na]

Fmoc-*endo*-dimethylcyclopropyl-Lys-OH·TFA (10).[32]—Fmoc amino acid **9** (40 mg, 0.083 mmol) in 1 mL of dichloromethane was cooled to 0 °C while stirring. 1 mL of trifluoroacetic acid was added and stirred for 15 minutes before being allowed to warm to 25 °C over 45 minutes. The reaction was concentrated *in vacuo* to an oil and residual solvent was removed by high vacuum over 2 hours. The amine was dissolved in 1.5 mL of acetonitrile followed by the addition of formaldehyde (37% w/w Aq, 12.5 mg, 0.415 mmol). Sodium cyanoborohydride (15.6 mg, 0.249 mmol) was added as one portion and stirred 5 minutes. Glacial acetic acid was added drop-wise to keep the pH 4–5. The reaction stirred 15 hours before being concentrated *in vacuo* to an oil and purified by RP-HPLC on a prep scale column

using a H_2O: Acetonitrile gradient with 0.05% trifluoroacetic acid to yield 30 mg (70%) of **10** as a white powder following lyophilization. ^1H (CD_3Cl_3, 400 MHz): δ 7.72 (d, 2H); 7.55 (t, 2H); 7.35 (t, 2H); 7.26 (t, 2H); 5.93 (d, 1H); 4.40 (m, 1H); 4.30 (d, 2H); 4.14 (t, 1H); 2.79 (bs, 6H); 2.29 (m, 1H); 2.00 (m, 1H); 1.80 (m,1H); 1.50 (m, 2H); 1.22 (m, 2H); 0.68 (m, 1H). HRMS: expected: 409.20, observed: 409.2118 [M+H]

(*S*)-dibenzyl 2-(dibenzylamino)pentanedioate (11).[28]—Glutamic acid (12.4 g, 84.2 mmol), potassium carbonate (46.5 g, 337 mmol), and potassium hydroxide (9.5 g, 168 mmol) in 125 mL of H_2O was brought to reflux while stirring. Benzyl bromide (50.0 mL, 421 mmol) was added drop-wise over 30 minutes and allowed to reflux an additional 30 minutes. The cooled reaction was extracted with diethyl ether 3 × 75 mL. The pooled organics were washed with saturated brine 2 × 50 mL. The organic phase was washed 2 × 75 mL with brine and dried over $MgSO_4$, filtered, and concentrated *in vacuo* to an oil. The crude product was purified by silica gel column chromatography in hexane: ethyl acetate (99:1-80:20) to yield 17 g (56%) of **11** as a clear viscous oil.[28] ^1H (CD_3Cl_3, 400 MHz): δ 7.41-7.19 (m, 20H); 5.21 (q, *J* = 30.4 and 12.4 Hz, 2H); 4.98 (q, *J* = 12.4 and 5.2 Hz, 2H); 3.88 (d, *J* = 14 Hz, 2H); 3.49 (d, *J* = 14 Hz, 2H); 3.41 (t, *J* = 7.6 Hz, 1H); 2.51 (m, 1H); 2.35 (m, 1H); 2.06 (q, *J* = 7.2 Hz, 2H).

(*S*)-benzyl 2-(dibenzylamino)-5-hydroxypentanoate (12).[28]—The benzyl protected amino acid **11** (19 g, 37.4 mmol) in 200 mL of anhydrous tetrahydrofuran was cooled to −10 °C with an ice/acetone bath while stirring under an argon atmosphere. DIBAL (1M in toluene, 112 mL, 112 mmol) was added drop-wise over 40 minutes. Following the addition, the reaction was warmed to 0 °C with an ice water bath and stirred 100 minutes. The reaction was quenched by the addition of 80 mL of H_2O and stirred an addition 20 minutes before being filtered through a pad of celite. The filtrate was dried over $MgSO_4$, filtered, and concentrated *in vacuo* to an oil. The crude product was purified by silica gel column chromatography in petroleum ether: diethyl ether (90:10-50:50) to yield 12 g (80%) of **12** as a clear viscous oil.[28] ^1H (CD_3Cl_3, 400 MHz): δ 7.45-7.21 (m, 15H); 5.21 (q, *J* = 31.5 and 12 Hz, 2H); 3.91 (d, *J* = 14 Hz, 2H); 3.51 (d, *J* = 14 Hz, 2H); 3.48 (q, *J* = 5.8 Hz, 2H); 3.38 (t, *J* = 7.6 Hz, 1H); 1.81 (m, 2H); 1.71 (m, 2H) 1.48 (m, 2H).

(*S*)-benzyl 2-(dibenzylamino)-5-oxopentanoate (13).[28]—Oxalyl chloride (2.25 ml, 25.8 mmol) in 140 mL anhydrous dichloromethane at −78 °C had DMSO (3.65 mL, 51.5 mmol) added drop-wise and stirred 25 minutes under an argon atmosphere. Alcohol **12** (5.2 g, 12.9 mmol) in 50 mL of anhydrous dichloromethane was added drop-wise to this solution and stirred an additional 30 minutes. Triethylamine (8.6 mL, 61.8 mmol) was added to the reaction and stirred 30 minutes at −78 °C, triethylamine (8.6 mL, 61.8 mmol) was again added to the reaction and allowed to warm to 0 °C over 30 minutes. 100 mL of H_2O was added to quench the reaction while warming to 25 °C. The organic phase was separated and the aqueous phase was extracted 2 × 100 mL with dichloromethane. The pooled organics were washed 1 × 75 mL with saturated sodium bicarbonate and saturated brine, dried over $MgSO_4$, filtered, and concentrated *in vacuo* to a golden oil. Residual solvent was removed by high vacuum over 2 hours. The product aldehyde was used without further purification yielding 5.0 g (97%) of **13** as an oil.[28] ^1H (CD_3Cl_3, 400 MHz): δ 9.59 (s, 1H); 7.43-7.23 (m, 15H); 5.23 (q, *J* = 27.6 and 12 Hz, 2H); 3.87 (d, *J* = 13.6 Hz, 2H); 3.50 (d, *J* = 13.6 Hz, 2H); 3.35 (t, *J* = 7.8 Hz, 1H); 2.53 (m, 1H); 2.42 (m, 1H); 2.03 (m, 2H); 1.55 (m, 2H).

(*S*,*E*)-7-benzyl 1-*tert*-butyl 6-(dibenzylamino)hept-2-enedioate (14).[29]—*tert*-butyl diethylphosphonoacetate (4.4 mL, 18.7 mmol) was added drop-wise to a stirring suspension of sodium hydride (60% dispersion in oil, 717 mg, 18.7 mmol) in 50 mL of anhydrous tetrahydrofuran at 0 °C under an argon atmosphere. The reaction is allowed to warm to 25 °C over 30 minutes before being cooled to −10 °C with an ice/acetone bath. Aldehyde **13** (5.0 g,

12.5 mmol) in 50 mL of anhydrous tetrahydrofuran was added drop-wise to the solution and stirred 30 minutes. After the solvent was removed *in vacuo*, the oil was partitioned in 100 mL of H_2O and diethyl ether. The aqueous phase was extracted 1 × 50 mL with diethyl ether. The pooled organics were washed 1 × 50 mL with saturated sodium bicarbonate and saturated brine, dried over $MgSO_4$, filtered, and concentrated *in vacuo* to a golden oil. The crude product was purified by silica gel column chromatography in petroleum ether: diethyl ether (99:1-90:10) to yield 5.3 g (85%) of **14** as a slightly yellow oil.[29] ^1H (CD_3Cl_3, 400 MHz): δ 7.44-7.20 (m, 15H); 6.70 (dt, *J* = 15.2 and 6.8 Hz, 1H); 5.58 (dt, *J* = 15.2 and 1.2 Hz); 5.21 (q, *J* = 28.7 and 12 Hz, 2H); 3.88 (d, *J* = 14 Hz, 2H); 3.50 (d, *J* = 14 Hz, 2H); 3.34 (t, *J* = 7.6 Hz, 1H); 2.32 (m, 1H); 2.05 (m, 1H); 1.86 (m, 2H); 1.46 (s, 9H). HRMS: expected: 500.27 [M+H], observed: 500.2799 [M+H]

***tert*-butyl 2-((*S*)-4-(benzyloxy)-3-(dibenzylamino)-4-oxobutyl)cyclopropane carboxylate (15).[30]—**Unsaturated *tert*-butyl ester **14** (5.25 g, 10.5 mmol) in 2:1 anhydrous dichloromethane: anhydrous diethyl ether was cooled to 0 °C while stirring under an argon atmosphere. Palladium(II) acetate (17.7 mg, 0.079 mmol) was added as one portion and stirred 5 minutes. Diazomethane (estimated at 0.37M in diethyl ether, 100 mL, 37 mmol) (see below for diazomethane generation procedure) was added drop-wise over 35 minutes via liquid addition funnel. The reaction was allowed to warm to 25 °C while stirring overnight. The reaction was filtered through a plug of celite and concentrated *in vacuo* to a golden oil. Residual solvent was removed by high vacuum over 3 hours. The cyclopropyl *tert*-butyl ester was used without further purification yielding 5.3 g (98%) of **15** as an oil. ^1H (CD_3Cl_3, 400 MHz): 2 predominant rotamers present δ 7.42-7.20 (m, 15H); 5.20 (q, J = 33.2 and 12 Hz, 2H); 3.89 (d, J = 14 Hz, 2H); 3.50 (d, J = 14 Hz, 2H); 3.35 (t, J = 7.6 Hz, 1H); 1.83 (m, 2H); 1.42 (s, 9H); 1.29 (m, 1H); 1.17 (m, 2H); 1.12 (m, 1H); 0.96 (m, 1H); 0.47 (m, 1H). HRMS: expected: 514.29 [M+H], observed: 514.2955 [M+H]

diazomethane—Diazomethane was generated according to Aldrich technical bulletin AL-180 in an Aldrich mini diazald apparatus. Diazald (5.0 g, 23 mmol) in 45 mL of diethyl ether was added drop-wise over 20 minutes to a 65 °C stirring solution of potassium hydroxide (2.5 g, 44.6 mmol) in 4 mL of H_2O, 8 mL of diethyl ether, and 14 mL of 2-(2-ethoxyethoxy) ethanol. The intensely yellow colored distillate is collected and stored at −78 °C in a brown bottle and used within 2 hours.

2-((*S*)-4-(benzyloxy)-3-(dibenzylamino)-4-oxobutyl)cyclopropanecarboxylic acid (16)—Cyclopropyl *tert*-butyl ester **15** (5.3 g, 10.3 mmol) in 100 mL of dichloromethane was cooled to 0 °C while stirring. 100 mL of trifluoroacetic acid was added and stirred for 15 minutes before being allowed to warm to 25 °C over 45 minutes. The solvent was removed *in vacuo*, and the oil partitioned in 100 mL of H_2O and dichloromethane. The aqueous phase was extracted 2 × 25 mL with dichloromethane. The pooled organics were washed 1 × 50 mL with saturated brine, dried over $MgSO_4$, filtered, and concentrated *in vacuo* to an oil. Residual solvent was removed by high vacuum over 2 hours. The carboxylic acid was used without further purification yielding 4.7 g (99%) of **16** as an oil. ^1H (CD_3Cl_3, 400 MHz): δ 7.43-7.20 (m, 15H); 5.21 (q, J = 28.4 and 12 Hz, 2H); 3.90 (d, J = 14 Hz, 2H); 3.54 (d, J = 14 Hz, 2H); 3.36 (t, J = 7.2 Hz, 1H); 1.84 (m, 2H); 1.43 (m, 1H); 1.32 (m, 1H); 1.25 (m, 2H); 1.10 (m, 1H); 0.62 (m, 1H). HRMS: expected: 458.23 [M+H], observed: 458.2326 [M+H]

(2*S*)-benzyl 4-(2-(*tert*-butoxycarbonylamino)cyclopropyl)-2-(dibenzylamino) butanoate (17).[31]—Acid **16** (4.7 g, 10.3 mmol) in 100 mL of anhydrous toluene was cooled to 0 °C while stirring under an argon atmosphere. Triethylamine (4.25 mL, 30.9 mmol) and diphenylphosphorylazide (4.54 mL, 21.0 mmol) were added and the reaction warmed to 25 °C over 3 hours. The reaction was washed 3 × 50 mL with H_2O, 1 × 25 mL with saturated brine,

dried over $MgSO_4$, filtered, and concentrated *in vacuo*. Residual solvent was removed by high vacuum over 4 hours. The azide was dissolved in 100 mL of anhydrous *tert*-butanol while stirring under an argon atmosphere and heated to reflux for 18 hours. The reaction was cooled to 25 °C and concentrated *in vacuo* to a golden oil. The oil was partitioned between 100 mL of H_2O and dichloromethane. The organic phase was washed 1 × 25 mL with saturated sodium bicarbonate and saturated brine, dried over $MgSO_4$, filtered, and concentrated *in vacuo*. The crude product was purified by silica gel column chromatography in petroleum ether: diethyl ether (95:5-60:40) to yield 3.6 g (66%) of **17** as a clear oil. ^1H (CD_3Cl_3, 400 MHz): δ 7.44-7.20 (m, 15H); 5.21 (q, J = 32.8 and 12 Hz, 2H); 3.89 (d, J = 14 Hz, 2H); 3.49 (d, J = 14 Hz, 2H); 3.38 (t, J = 7.6 Hz, 1H); 2.13 (m, 1H); 1.84 (m, 2H); 1.44 (s, 9H); 1.38 (m, 1H); 1.18 (m, 1H); 0.55 (m, 1H); 0.49 (m, 1H); 0.37 (m, 1H). HRMS: expected: 529.30 [M+H], observed: 529.3064 [M+H]

hydrazino-Lys-4 H3-21 (18)—Lyophilized mesyl-Lys-4 H3-21 (**5**) (5.0 mg, 2.1 μmol) was dissolved in 750 μL of 1:1 H_2O:CH_3CN. Hydrazine monohydrate (57 μL, 860 μmol) was added to the solution and rotated 70 hours at 25 °C. The crude reaction mixture was diluted to 3 mL with H_2O, acidified to pH 2 with TFA, and injected onto a prep scale column for RP-HPLC purification. Analysis by MALDI-TOF showed an expected/observed *m/z* = 2269.33.

Enzyme Expression and Purification

LSD1 (aa 171–852) subcloned into the pGEX-6P-1 vector (GE Healthcare) was overexpressed in *E. coli* BL21-CodonPlus®(DE3)-RIPL cells (Stratagene).[22] Cells were grown to an $OD_{600\ nm}$ of 1.8 in CircleGrow® Media (Q-Biogene) at 37 °C then induced with 1 mM final IPTG and grown for 20 hours at 16 °C. Cell pellets were harvested by centrifugation at 5000 × g for 15 minutes and resuspended in ice cold lysis buffer (280 mM NaCl, 5.4 mM KCl, 20 mM Na_2HPO_4, 3.6 mM KH_2PO_4, 1 mM EDTA, 10 mM DTT, 10% glycerol, pH 7.4). The cells were then lysed via double pass on a French press (16,000–18,000 psi), and the lysates clarified by centrifugation at 25,000 × g for 30 minutes. The clarified lysate from 1 L of culture was double loaded (0.5 mL/min) onto a 5 mL glutathione sepharose 4 fast flow column (GE Healthcare) that was pre-equilibrated with lysis buffer. The column was then washed with 75 mL of lysis buffer and eluted with 5 × 5 mL fractions of lysis buffer containing 50 mM reduced glutathione (Sigma). GST-LSD1 containing fractions were pooled and dialyzed against 3 × 1 L changes of lysis buffer containing 1 mM β-mercaptoethanol instead of 10 mM DTT. The dialyzed protein was concentrated to 1–2 mL and further purified by size exclusion chromatography using sephacryl S100 high resolution media (GE Healthcare, 1.5 × 90 cm column). The protein was eluted with lysis buffer containing 1 mM β-mercaptoethanol instead of 10 mM DTT at a flow rate of 0.25 mL/min. GST-LSD1 containing fractions were pooled, concentrated, aliquoted, and stored at −80 °C. Final protein concentration was determined by Bradford assay using BSA as the standard. Purification of GST-LSD1 by this procedure yielded approximately 1 mg of protein (>90% pure) per 1 L of culture.

LSD1 Activity Assays

Initial velocity measurements were performed using a peroxidase-coupled assay, which monitors hydrogen peroxide production as previously described.[21] The time courses of the reaction were measured under aerobic conditions using a Beckman Instruments DU series 600 spectrophotometer equipped with a thermostated cell holder (*T* = 25 °C). The 150 μL reactions were initiated by the addition of 50 μl of buffered substrate (dimethyl-Lys-4 H3-21) solution to reaction mixtures (100 μl) consisting of 50 mM HEPES buffer (pH 7.5), 0.1 mM 4-aminoantipyrine, 1 mM 3,5-dichloro-2-hydroxybenzenesulfonic acid, 0.76 μM horseradish peroxidase (Worthington Biochemical Corporation), and 185 nM GST-LSD1. Absorbance changes were monitored at 515 nm, and an extinction coefficient of 26,000 M^{-1} cm^{-1} was used to calculate product formation. Under these conditions, GST-LSD1 displayed at k_{cat} of 4.5 ±

0.1 min^{-1} and a K_m for dimethyl-Lys-4 H3-21 of 21 ± 2 μM. A secondary assay was necessary in the case of inactivator **18**. In this case, the 150 μL reactions were initiated by the addition of 50 μl of buffered substrate (dimethyl-Lys-4 H3-21) solution to reaction mixtures (100 μl) consisting of 50 mM HEPES buffer (pH 7.5), 0.1 mM Amplex® Red, 0.76 μM horseradish peroxidase, and 25 nM LSD1. Absorbance changes were monitored at 571 nm, and an extinction coefficient of 52,000 M^{-1} cm^{-1} was used to calculate product formation. Under these conditions, our GST-LSD1 displayed at k_{cat} of 3.5 ± 0.2 min^{-1} and a K_m for dimethyl-Lys-4 H3-21 of 20 ± 3 μM.

Inhibition Studies

Inhibitors were tested by using the peroxidase-coupled assay described above. In these experiments, assays were initiated by the addition of buffered substrate and the inhibitor simultaneously. Final substrate concentrations were 60 μM (3× K_m when examining **7**), 100 μM (5× K_m when examining **8**), 240 μM (12× K_m when examining **3**,**4**, and phenelzine) or 600 μM (30× K_m when examining **18**). With the exception of the evaluation of **18**, GST-LSD1 was present at 185 nM. Inactivator peptide **18** required a more sensitive assay and was analyzed using Amplex® Red as the horseradish peroxidases co-substrate rather than 4-aminoantipyrine and 3,5-dichloro-2-hydroxybenzenesulfonic acid as noted previously, LSD1 was present in these assays at 25 nM. Progress curves obtained in the presence of inactivators **3**, **4**, **18** and phenelzine were fit to the following single exponential for slow-binding inhibitors which assumes a steady-state velocity of zero:[41]

$$\text{Product} = v_0(1 - e^{-kt})/k + \text{offset} \quad \text{(Eq. 1)}$$

The k_{obs} values were then analyzed by the method of Kitz and Wilson to yield k_{inact} and $K_{i(inact)}$. The following equation was used to extract kinetic constants from the Kitz-Wilson analysis:[42]

$$k_{obs} = (k_{inact} * [I])/(K_{i(inact)} + [I]) \quad \text{(Eq. 2)}$$

$K_{i(inact)}$ was extrapolated to zero substrate by:

$$K_{i(inact)}^{app} = K_{i(inact)} * (1 + S/K_m) \quad \text{(Eq. 3)}$$

The $t_{1/2}$ for inactivation at saturation was obtained by:

$$t_{1/2} = (\ln 2)/k_{inact} \quad \text{(Eq. 4)}$$

Compounds **7** and **8** did not display time-dependent inhibition. Initial velocities at increasing concentrations of **7** and **8** were obtained by linear regression to reaction progress curves. These velocities were used to determine the K_i for **7** and **8** by Dixon analysis assuming competitive inhibition. The K_i was extrapolated to zero substrate by:

$$K_i^{app} = K_i * (1 + S/K_m) \quad \text{(Eq. 5)}$$

Adduct Analysis by Absorbance Spectroscopy

GST-LSD1 (4.25 μM) was incubated with potential inactivators (30 μM), or no inhibitor in 50 mM HEPES (pH 7.5) at 25 °C. After 1 hour, the samples were clarified by centrifugation at

14,000 × g for 10 minutes (25 °C) and the flavin absorbance spectra was recorded (350–550 nm).

MALDI-TOF Mass Spectrometric Analysis of Peptide Inactivators

Aliquots of the GST-LSD1 that was inactivated by peptides **3**,**4** and **18** in the absorbance spectroscopic analysis above were used for MALDI-TOF mass spectrometric analysis. The sample was applied to a C_{18} ZipTip® (Millipore) column, and eluted with 75:25 CH_3CN:H_2O containing 0.05% TFA. The eluent was analyzed by MALDI-TOF mass spectrometry in α-cyano-4-hydroxycinnamic acid.

Preincubation Assay with Phenelzine

GST-LSD1 (10 μM) was incubated with phenelzine (250 μM), or no inhibitor, in 50 mM HEPES (pH 7.5) for 30 minutes at 25 °C. The inhibition study described above was initiated by the addition of 3 μL of preincubated LSD1 to reaction mixtures consisting of substrate and cosubstrates for a final phenelzine concentration of 5 μM in 150 μL. Two control assays were performed, the first lacking phenelzine and the second consisting of phenelzine present in the reaction mixture for 5 μM final.

MALDI-TOF Preincubation Analysis with Phenelzine

GST-LSD1 (185 nM) was incubated with phenelzine (500 μM), or no inhibitor, in 50 mM HEPES (pH 7.5) at 25 °C. After 30 minutes dimethyl-Lys-4 H3-21 substrate (10 μM final) was added and incubated for 30 addition minutes. Each sample was applied to a C_{18} ZipTip® (Millipore) column, and eluted with 1:1 CH_3CN:H_2O containing 0.05% TFA. The eluent was analyzed by MALDI-TOF mass spectrometry in α-cyano-4-hydroxycinnamic acid.

Antibodies

Antibodies against mono-, di, and trimethylated H3K4 were obtained from Abcam (Cambridge, MA).

Cell Culture, Transient Transfection, and Reporter Analyses

Monolayer cultures of clone −23 cells derived from GH3 cells and containing a luciferase reporter construct under the control of the TSH -subunit promoter (−840 to +1),[38] were grown in DMEM (Life Technologies, Inc., Gaithersburg, MD) supplemented with 10% heat-inactivated fetal calf serum (Biofluids, Rockville, MD) and maintained in 5% CO_2 atmosphere at 37 °C. Cells were transfected with 300 ng DNA/well in 12-well plates with Lipofectamine 2000 (Invitrogen) according to the manufacturer's instructions. Cell culture media were changed 6 hours after transfection to antibiotic-free DMEM plus 10% charcoal-dextran-treated fetal bovine serum. T_3 was added to the cells 48 hours later, and cells were harvested, lysed and assayed for reporter gene activity the next day using dual luciferase assay reagents according to the manufacturer's instructions (Promega Corp., Madison, WI).

Chromatin Immunoprecipitation (ChIP) Assay

ChIP assay was performed as previously described.[38] α-23 cells were grown to 90% confluence in phenol red-free DMEM supplemented with 10% charcoal DEXTRAN-stripped fetal bovine serum (FBS) for 3 days. After addition of 10^{-6} M T_3 and/or 10 μM phenelzine for one hour, ChIP assays were performed according to manufacturer's protocol (Upstate Biotechnology) with some minor modifications. After treatment with T_3, chromatin was cross-linked with 1% formaldehyde in PBS, and nuclei extracted. Chromatin was sonicated to generate 500- to 1000-bp DNA fragments, and the supernatant containing precleared chromatin was incubated at 0 °C overnight with different antibodies or rabbit IgG control. After reverse cross-linking by

heating the samples at 65 °C overnight, and treating with Proteinase K, DNA was purified with a QIAGEN PCR Purification Kit (QIAGEN, Chatsworth, CA) according to the manufacturer's instructions. Quantitative real-time PCR of ChIP products was performed using primers that amplified the promoter region of TSH in pGL2/TSH (upstream primer: 5-CAGGATGTTATGTGTATGGCTC- 3' and downstream primer: 5'-CTTTATGTTTTTGGCGTCTTC-3'). We employed the SYBR green system (Applied Biosystems) using an Applied Biosystems 7300 sequence detector. Relative values (mean ± SD) normalized to input levels were compared with those obtained with control IgG.

Acknowledgments

We thank the NIH for financial support and L. Szewczuk for helpful suggestions.

References

1. Taverna SD, Li H, Ruthenburg AJ, Allis CD, Patel DJ. How chromatin-binding modules interpret histone modifications. Nat. Struct. Mol. Biol 2007;14:1025–1040. [PubMed: 17984965]
2. Cole PA. Chemical probes for histone-modifying enzymes. Nat. Chem. Biol 2008;4:590–597. [PubMed: 18800048]
3. Martin C, Zhang Y. The diverse functions of histone lysine methylation. Nat. Rev. Mol. Cell. Biol 2005;6:838–849. (2005). [PubMed: 16261189]
4. Kouzarides T. Chromatin modifications and their function. Cell 2007;282:15040–15047.
5. Shi Y, Lan F, Matson C, Mulligan P, Whetstine JR, Cole PA, Casero RA, Shi Y. Histone demethylation mediated by the nuclear amine oxidase homolog LSD1. Cell 2004;119:941–953. [PubMed: 15620353]
6. Tsukada Y, Fang J, Erdjument-Bromage H, Warren ME, Borchers CH, Tempst P, Zhang Y. Histone demethylation by a family of JmjC domain-containing proteins. Nature 2006;439:811–816. [PubMed: 16362057]
7. Karytinos A, Forneris F, Profumo A, Ciossani G, Battaglioli E, Binda C, Mattevi A. A novel mammalian flavin-dependent histone demethylase. J. Biol. Chem 2009;284:17775–17782. [PubMed: 19407342]
8. Binda C, Mattevi A, Edmonson DE. Structure-function relationships in flavoenzyme-dependent amine oxidations: a comparison of polyamine oxidase and monoamine oxidase. J. Biol. Chem 2002;277:23973–23976. [PubMed: 12015330]
9. Hakimi MA, Dong Y, Lane WS, Speicher DW, Shiekhattar R. A candidate X-linked mental retardation gene is a component of a new family of histone deacetylase-containing complexes. J. Biol. Chem 2003;278:7234–7239. [PubMed: 12493763]
10. Humphrey GW, Wang Y, Russanova VR, Hirai T, Qin J, Nakatani Y, Howard BH. Stable histone deacetylase complexes distinguished by the presence of SANT domain proteins. CoREST/kiaa0071 and Mta-L1. J. Biol. Chem 2001;276:6817–6824. [PubMed: 11102443]
11. Shi Y, Sawada J, Sui G, Affar el B, Whetstine JR, Lan F, Ogawa H, Luke MP, Nakatani Y, Shi Y. Coordinated histone modifications mediated by a CtBP corepressor complex. Nature 2003;422:735–738. [PubMed: 12700765]
12. You A, Tong JK, Grozinger CM, Schreiber SL. CoREST is an integral component of the CoREST-human histone deacetylase complex. Proc. Natl. Acad. Sci. U. S. A 2001;98:1454–1458. [PubMed: 11171972]
13. Forneris F, Binda C, Vanoni MA, Battaglioli E, Mattevi A. Human histone demethylase LSD1 reads the histone code. J. Biol. Chem 2005;280:41360–41365. [PubMed: 16223729]
14. Lee MG, Wynder C, Schmidt DM, McCafferty DG, Shiekhattar R. Histone H3 lysine 4 demethylation is a target of nonselective antidepressive medications. Chem. Biol 2006;13:563–567. [PubMed: 16793513]
15. Huang Y, Greene E, Stewart TM, Goodwin AC, Baylin SB, Woster PM, Casero RA Jr. Inhibition of lysine-specific demethylase 1 by polyamine analogues results in reexpression of aberrantly silenced genes. Proc. Natl. Acad. Sci. USA 2007;104:8023–8028. [PubMed: 17463086]

16. Edmondson DE, Mattevi A, Binda C, Li M, Hubálek F. Structure and mechanism of monoamine oxidase. Curr. Med. Chem 2004;11:1983–1993. [PubMed: 15279562]
17. Yu PH. Pharmacological and clinical implications of MAO-B inhibitors. Gen Pharmacol 1994;25:1527–1539. [PubMed: 7721026]
18. Goodman WK, Charney DS. Therapeutic applications and mechanisms of action of monoamine oxidase inhibitor and heterocyclic antidepressant drugs. J. Clin. Psychiatry 1985;46:6–24. [PubMed: 3900056]
19. Schmidt DM, McCafferty DG. trans-2-Phenylcyclopropylamine Is a mechanism-based inactivator of the histone demethylase LSD1. Biochemistry 2007;46:4408–4416. [PubMed: 17367163]
20. Yang M, Culhane JC, Szewczuk LM, Jalili P, Ball HL, Machius M, Cole PA, Yu H. Structural basis for the inhibition of the LSD1 histone demethylase by the antidepressant trans-2-phenylcyclopropylamine. Biochemistry 2007;46:8058–8065. [PubMed: 17569509]
21. Culhane JC, Szewczuk LM, Liu X, Da G, Marmorstein R, Cole PA. A mechanism-based inactivator for histone demethylase LSD1. J. Am. Chem. Soc 2006;128:4536–4537. [PubMed: 16594666]
22. Szewczuk LM, Culhane JC, Yang M, Majumdar A, Yu H, Cole PA. Mechanistic analysis of a suicide inactivator of histone demethylase LSD1. Biochemistry 2007;46:6892–6902. [PubMed: 17511474]
23. Yang M, Culhane JC, Szewczuk LM, Gocke CB, Brautigam CA, Tomchick DR, Machius M, Cole PA, Yu H. Structural basis of histone demethylation by LSD1 revealed by suicide inactivation. Nat. Struct. Mol. Biol 2007;14:535–539. [PubMed: 17529991]
24. Rando RR, Eigner A. The pseudoirreversible inhibition of monoamine oxidase by allylamine. Mol. Pharmacol 1997;13:1005–1013. [PubMed: 593260]
25. Jeon HB, Sayre LM. Highly potent propargylamine and allylamine inhibitors of bovine plasma amine oxidase. Biochem. Biophys. Res. Commun 2009;304:788–794. [PubMed: 12727226]
26. Woo JCG, Silverman RB. Observation of two different chromophores in the resting state of monoamine oxidase B by fluorescence spectroscopy. Biochem. Biophys. Res. Comm 1994;202:1574–1578. [PubMed: 8060341]
27. Brandl M, Kozhushkov SI, Loscha K, Kokoreva OV, Yufit DS, Howard JAK, de Meijere A. Synthesis of *trans*-(2-aminocyclopropyl)alanine – A key constituent of the novel antitumor antibiotic belactosin A. Synlett 2000;12:1741–1744.
28. Kokotos G, Padron JM, Martin T, Gibbons WA, Martin VS. A general approach to the asymmetric synthesis of unsaturated lipidic α-amino acids. The first synthesis of α-aminoarachidonic acid. J. Org. Chem 1998;63:3741–3744.
29. Barrett AGM, Head J, Smith ML, Stock NS, White AJP, Williams DJ. Fleming-Tamao oxidation and masked hydroxl functionality: Total synthesis of (+)-pramanicin and structural elucidation of the antifungal natural product (−)-pramanicin. J. Org. Chem 1999;64:6005–6018.
30. Tchilibon S, Kim SK, Gao ZG, Harris BA, Blaustein JB, Gross AS, Duong HT, Melman N, Jacobson KA. Exploring distal regions of the A_3 adenosine receptor binding site: Sterically constrained N^6-(2-phenylethyl)adenosine derivatives as potent ligands. Bioorg. Med. Chem 2004;12:2021–2034. [PubMed: 15080906]
31. Raju B, Anandan S, Gu S, Herradura P, O'Dowd H, Kim B, Gomez M, Hackbarth C, Wu C, Wang W, Yuan Z, White R, Trias J, Patel DV. Conformationally restricted analogs of deoxynegamycin. Bioorg. Med. Chem. Lett 2004;14:3103–3107. [PubMed: 15149653]
32. Arvidsson LE, Johansson AM, Hacksell U, Nilsson JLG, Svensson K, Hjorth S, Magnusson T, Carlsson A, Lindberg P, Andersson B, Sanchez D, Wikstrom H, Sundell S. *N*,*N*-Dialkylated monophenolic *trans*-2-phenelcyclopropylamines: Novel central 5-hydroxytryptamine agonists. J. Med. Chem 1988;31:92–99. [PubMed: 3336037]
33. Zhou M, Diwu Z, Panchuk-Voloshina N, Haugland RP. A stable nonfluorescent derivative of resorufin for the fluorometric determination of trace hydrogen peroxide: applications in detecting the activity of phagocyte NADPH oxidase and other oxidases. Anal. Biochem 1997;253:162–168. [PubMed: 9367498]
34. Clineschmidt BV, Horita A. The monoamine oxidase catalyzed degradation of phenelzine-1-^{14}C, an irreversible inhibitor of monoamine oxidase. Biochem. Pharmacol 1969;18:1011–1020. [PubMed: 4389278]

35. Yu PH, Tipton KF. Deuterium isotope effect of phenelzine on the inhibition of rat liver mitochondrial monoamine oxidase activity. Biochem. Pharmacol 1989;38:4245–4251. [PubMed: 2597196]

36. Ueda R, Suzuki T, Mino K, Tsumoto H, Nakagawa H, Hasegawa M, Sasaki R, Mizukami T, Miyata N. J. Am. Chem. Soc. asap 10.1021/ja907055q.

37. Patek DR, Hellerman L. Mitochondrial monoamine oxidase: mechanism of inhibition by phenylhydazine and by aralkylyhydrazines. J. Biol. Chem 1974;249:2373–2380. [PubMed: 4822496]

38. Wang D, Xia X, Liu Y, Oetting A, Walker RL, Zhu Y, Meltzer P, Cole PA, Shi YB, Yen PM. Negative regulation of TSHalpha target gene by thyroid hormone involves histone acetylation and corepressor complex dissociation. Mol. Endocrinol 2009;23:600–609. [PubMed: 19196836]

39. Jones PA, Baylin SB. The epigenomics of cancer. Cell 2007;128:683–692. [PubMed: 17320506]

40. Minucci S, Pelicci PG. Histone deacetylase inhibitors and the promise of epigenetic (and more) treatments for cancer. Nat. Rev. Cancer 2006;6:38–51. [PubMed: 16397526]

41. Copeland, RA. Enzymes: A Practical Introduction to Structure, Mechanism, and Data Analysis. 2nd Ed.. New York, New York: Wiley-VCH; 2000.

42. Kitz R, Wilson IB. Esters of methanesulfonic acid as irreversible inhibitors of acetylcholinesterase. J. Biol. Chem 1962;237:3245–3249. [PubMed: 14033211]

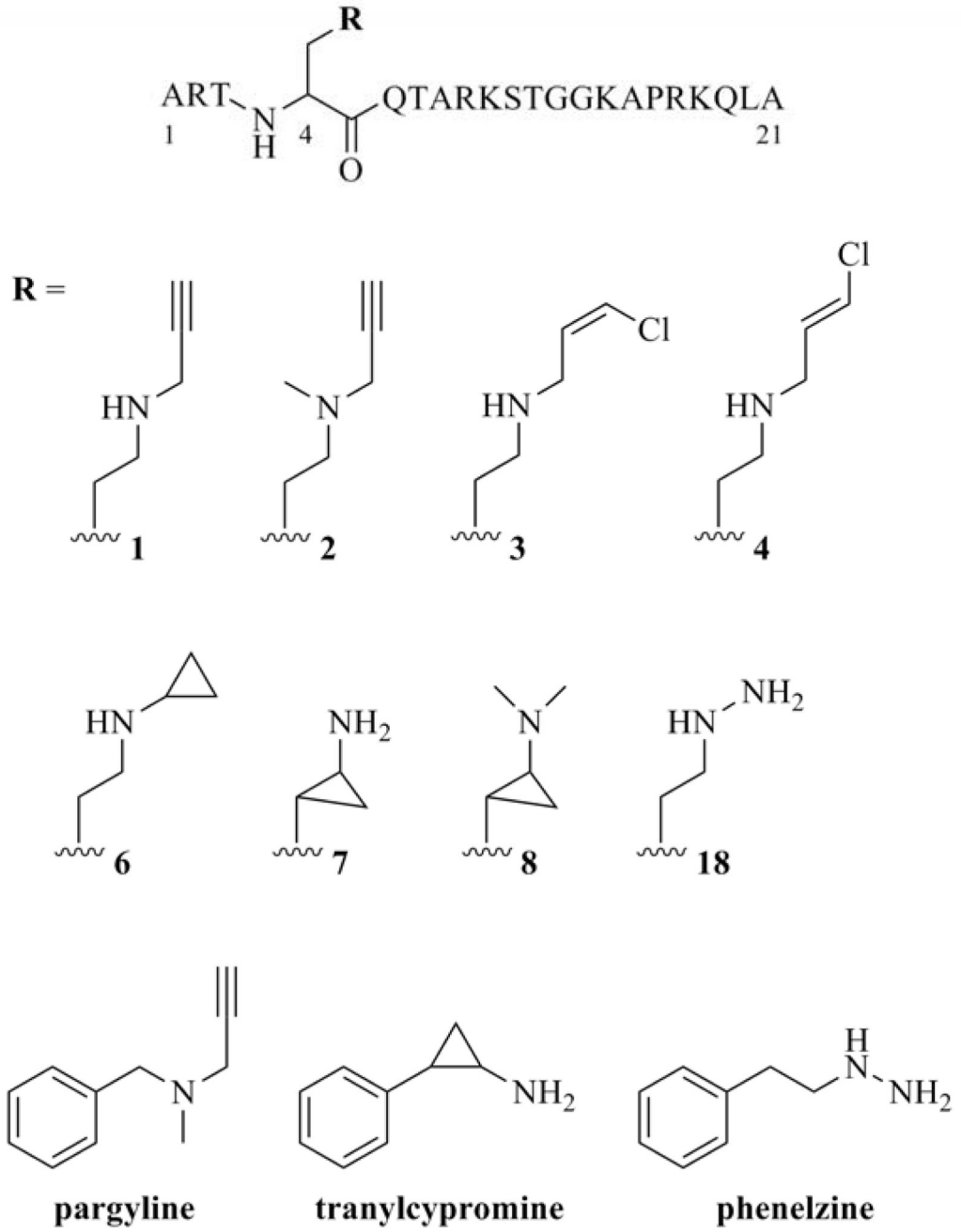

Figure 1.
Structures of evaluated GST-LSD1 inhibitors and inactivators.

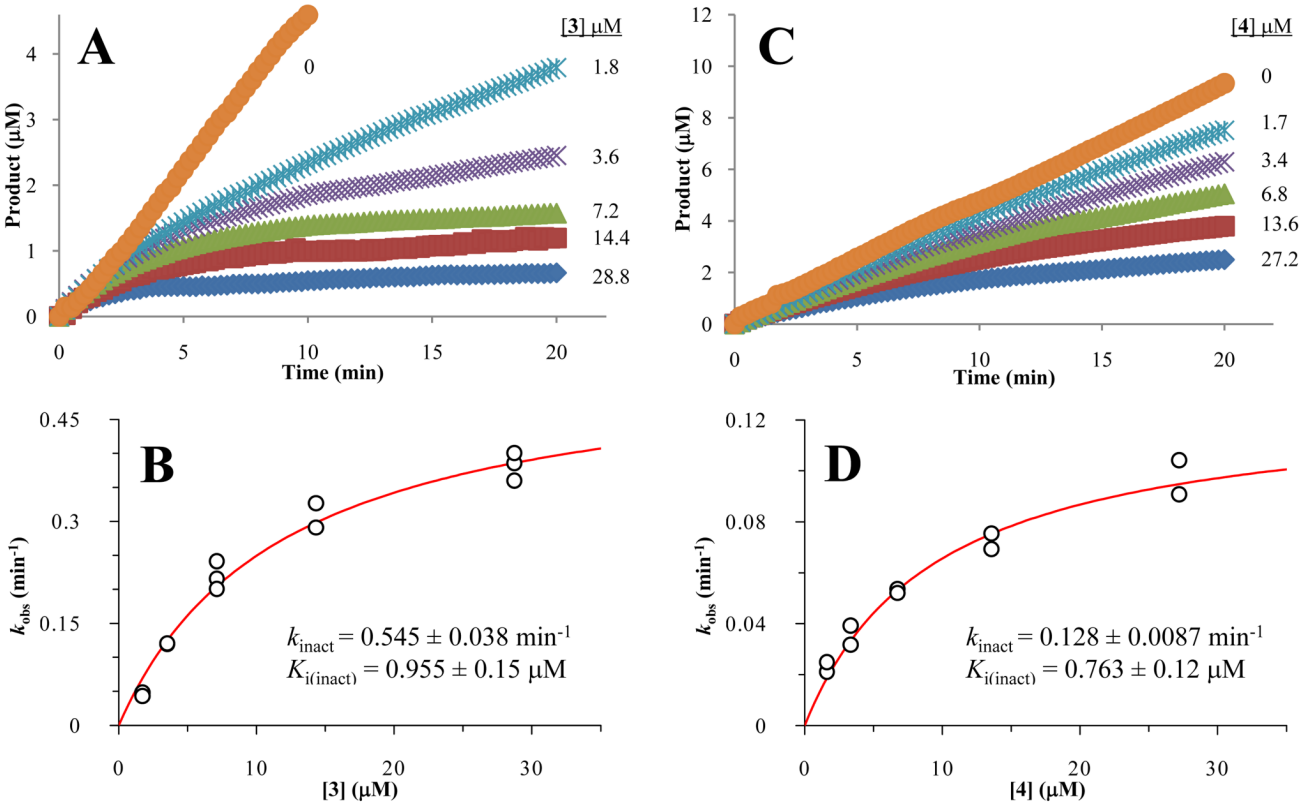

Figure 2.

Time- and concentration-dependent inactivation of GST-LSD1 by *cis*-3-chloroallyl-Lys-4 H3-21 (**3**) and *trans*-3-chloroallyl-Lys-4 H3-21 (**4**). A and C) Steady-state progress curves obtained for the inactivation of LSD1 in the presence of concentrations of **3** ranging from 0 to 28.8 μM and concentrations of **4** ranging from 0 to 27.2 μM. B and D) Rate constants (k_{obs}) for the time-dependent inactivation of LSD1 by **3** and **4** were extracted from the steady-state data in A and C by single exponential fits and analyzed by the method of Kitz and Wilson to determine k_{inact} and $K_{i(inact)}$ values.

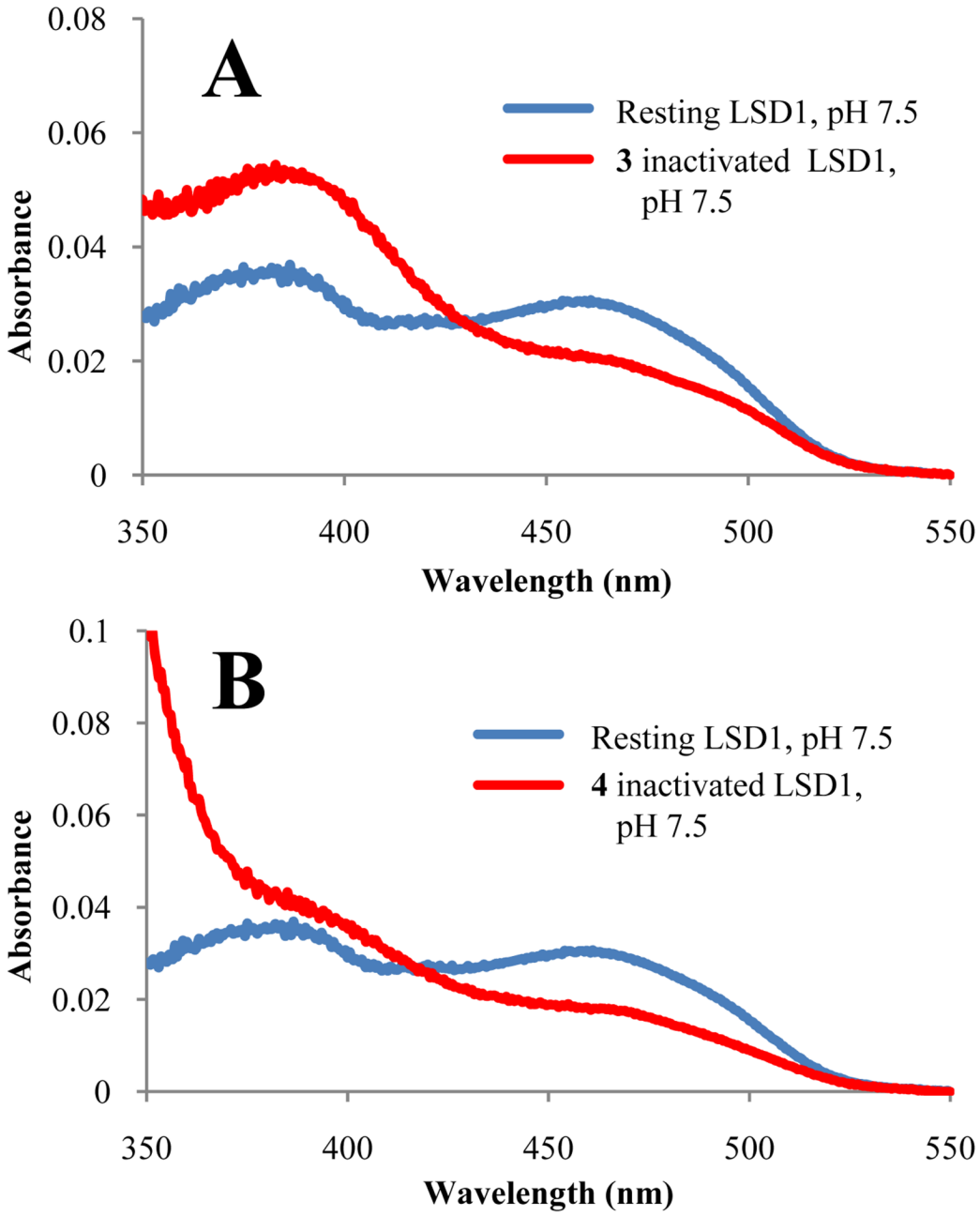

Figure 3.

Spectroscopic analysis of *cis* or *trans*-3-chloroallyl-Lys-4 H3-21 (**3** and **4**) treated GST-LSD1. UV/Vis spectra of native LSD1 (blue) shows the distinctive two maxima of the fully oxidized flavin and the one electron reduced semiquinone. A) LSD1 treated with **3** leads to a shift in the absorbance to a new maximum at 383 nm. B) LSD1 treated with **4** leads to a shift in the absorbance to a new maximum less than 350 nm.

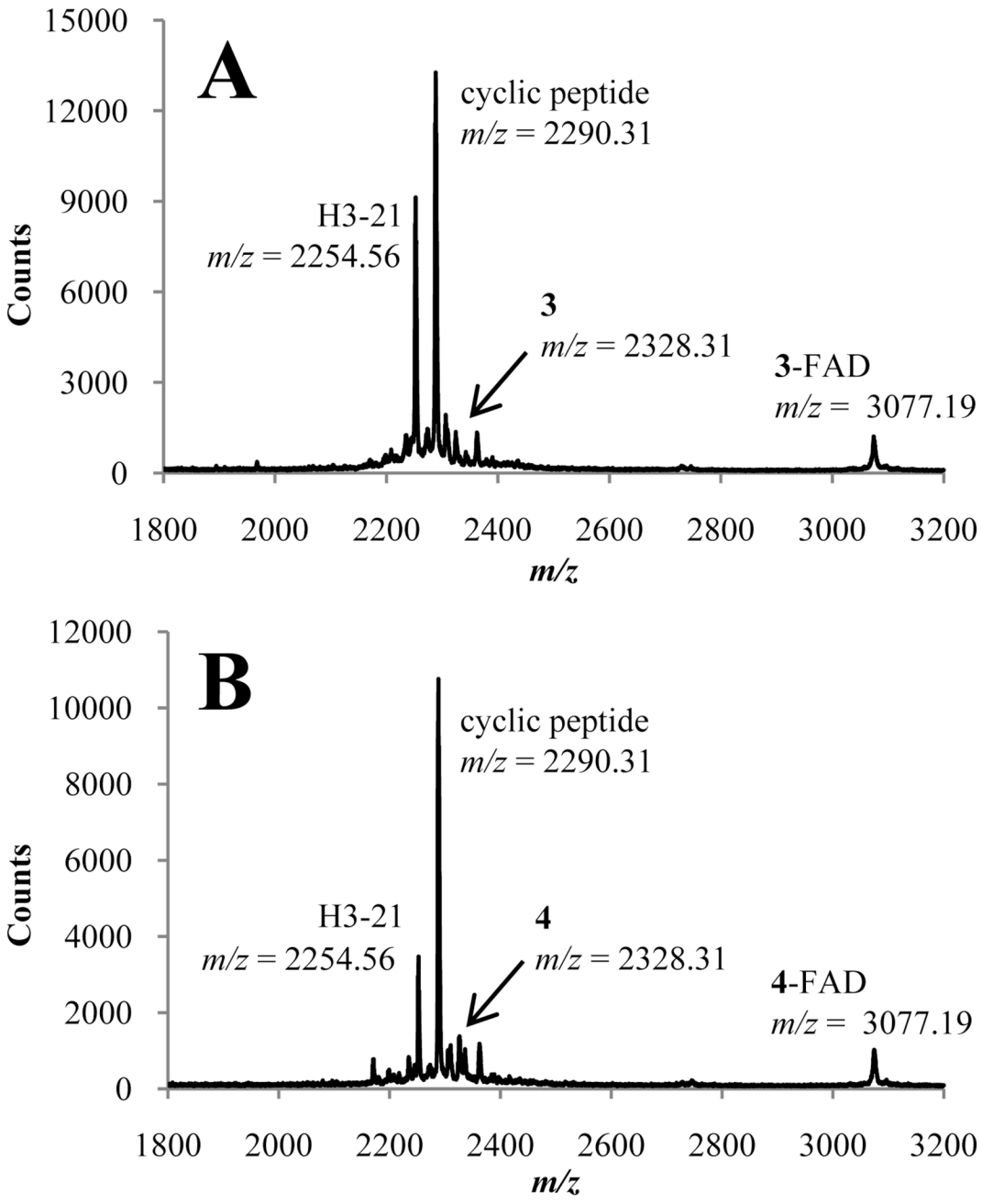

Figure 4.

MALDI-TOF analysis of GST-LSD1 incubated with *cis* or *trans*-3-chloroallyl-Lys-4 H3-21 (**3** and **4**). A) Inactivator **3** is seen as a minor peak, while a new signal corresponding to the predicted mass of a **3**-FAD adduct is now apparent. Additionally, a signal corresponding to the hydrolysis of **3**, forming H3-21 is noted. Possible intramolecular cyclization of the activated peptide is seen as the major peak. B) Inactivator **4** is seen as a minor peak, while a new signal corresponding to the predicted mass of a **4**-FAD adduct is now apparent. A signal corresponding to the hydrolysis of **4**, forming H3-21 is noted. Possible intramolecular cyclization of the activated peptide is seen as the major peak.

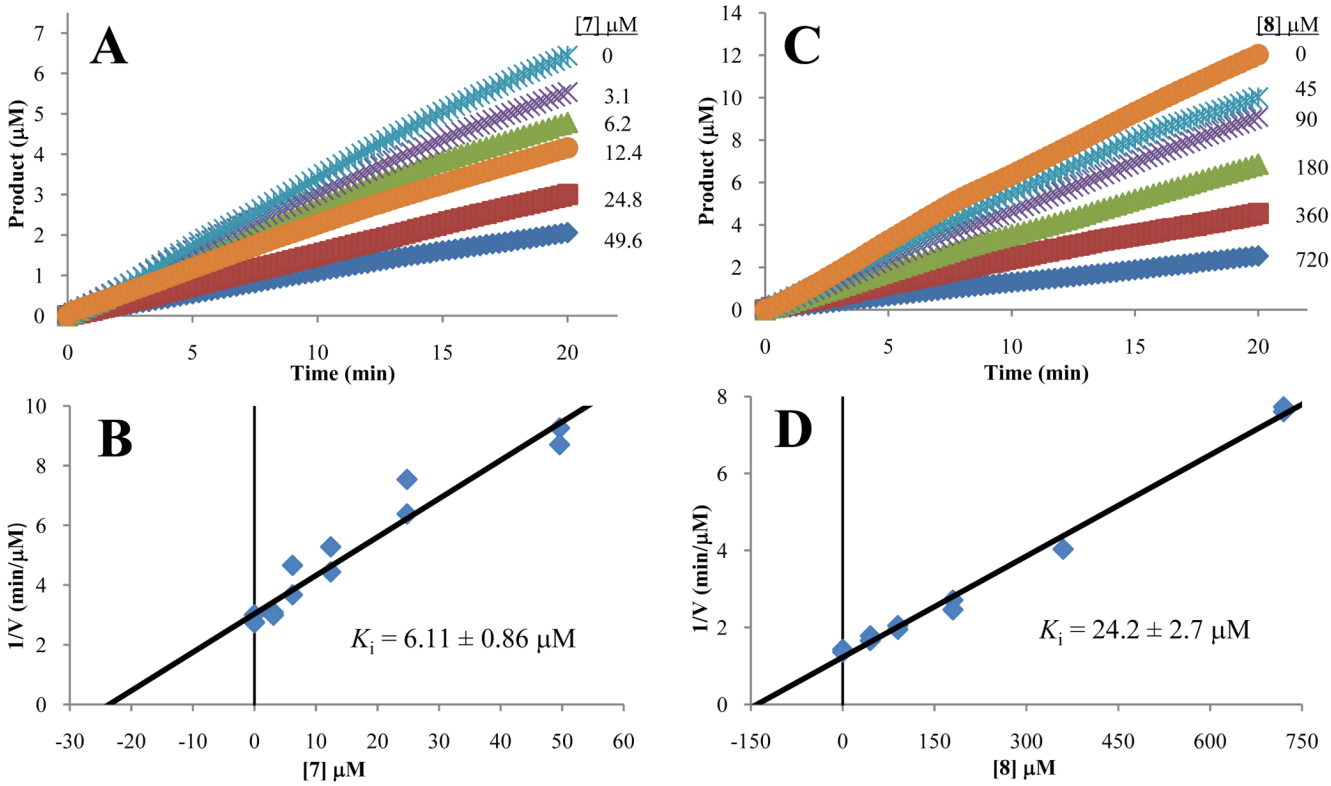

Figure 5.

Inhibition of GST-LSD1 by *endo*-cyclopropyl-Lys-4 H3-21 (**6**) and *endo*-dimethylcyclopropyl-Lys-4 H3-21 (**7**). A and C) Steady-state progress curves obtained for the inhibition of LSD1 in the presence of concentrations of **6** ranging from 0 to 49.6 μM and concentrations of **7** ranging from 0 to 720 μM. B and D) Steady-state velocities obtained in A and C were used to determine the K_i for compounds **6** and **7** by Dixon analysis.

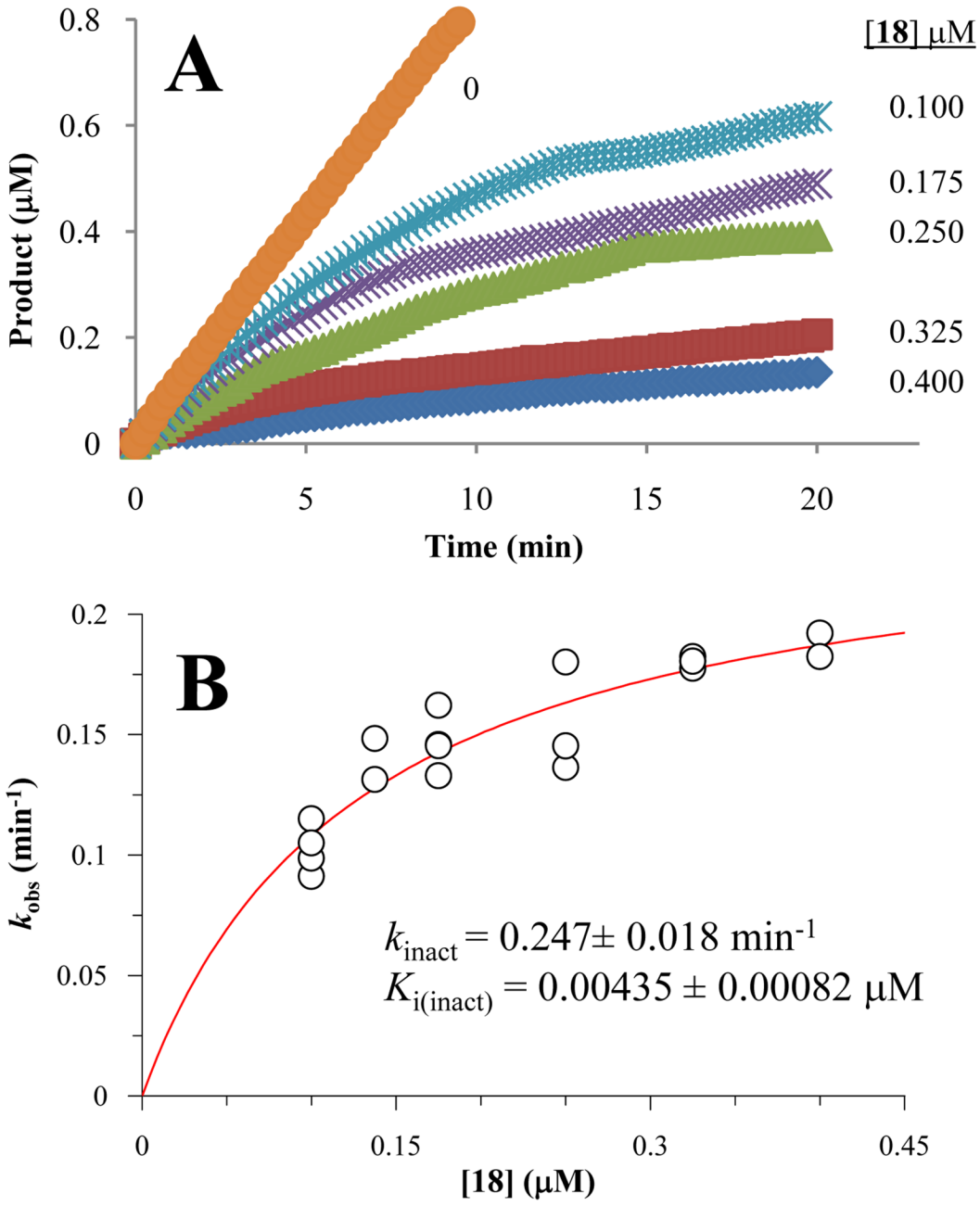

Figure 6.

Time- and concentration-dependent inactivation of GST-LSD1 by hydrazino-Lys-4 H3-21 (**18**). A) Steady-state progress curves obtained for the inactivation of LSD1 in the presence of concentrations of **18** ranging from 0.1 to 0.4 μM. B) Rate constants (k_{obs}) for the time-dependent inactivation of LSD1 by **18** were extracted from the steady-state data in A by single exponential fits and analyzed by the method of Kitz and Wilson to determine k_{inact} and $K_{i(inact)}$ values.

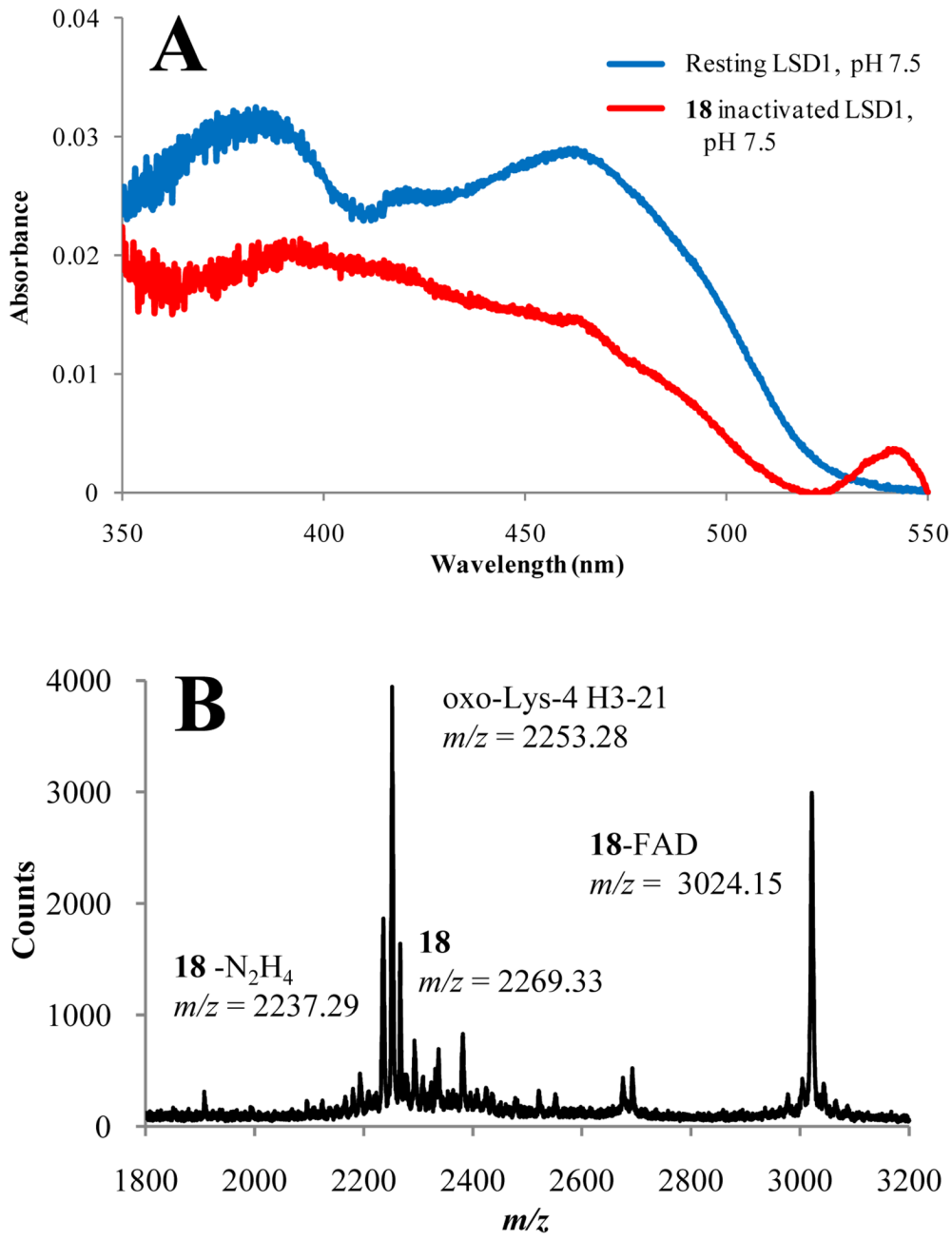

Figure 7.

Spectroscopic and MALDI-TOF analysis of hydrazino-Lys-4 H3-21 (**18**) treated GST-LSD1. A) UV/Vis spectra of native LSD1 (blue) shows the distinctive two maxima of the fully oxidized flavin and the one electron reduced semiquinone. LSD1 treated with **18** (red) leads to the bleaching of the flavin spectra with no new maximum recorded. B) In the MALDI-TOF analysis **18** is seen as a minor peak, while a major peak corresponding to the predicted mass of an **18**-FAD adduct is now evident. Additionally, a signal corresponding to the hydrolysis of **18**, forming the aldehyde containing peptide is noted along with a possible degradation to the olefin or intramolecular cyclization.

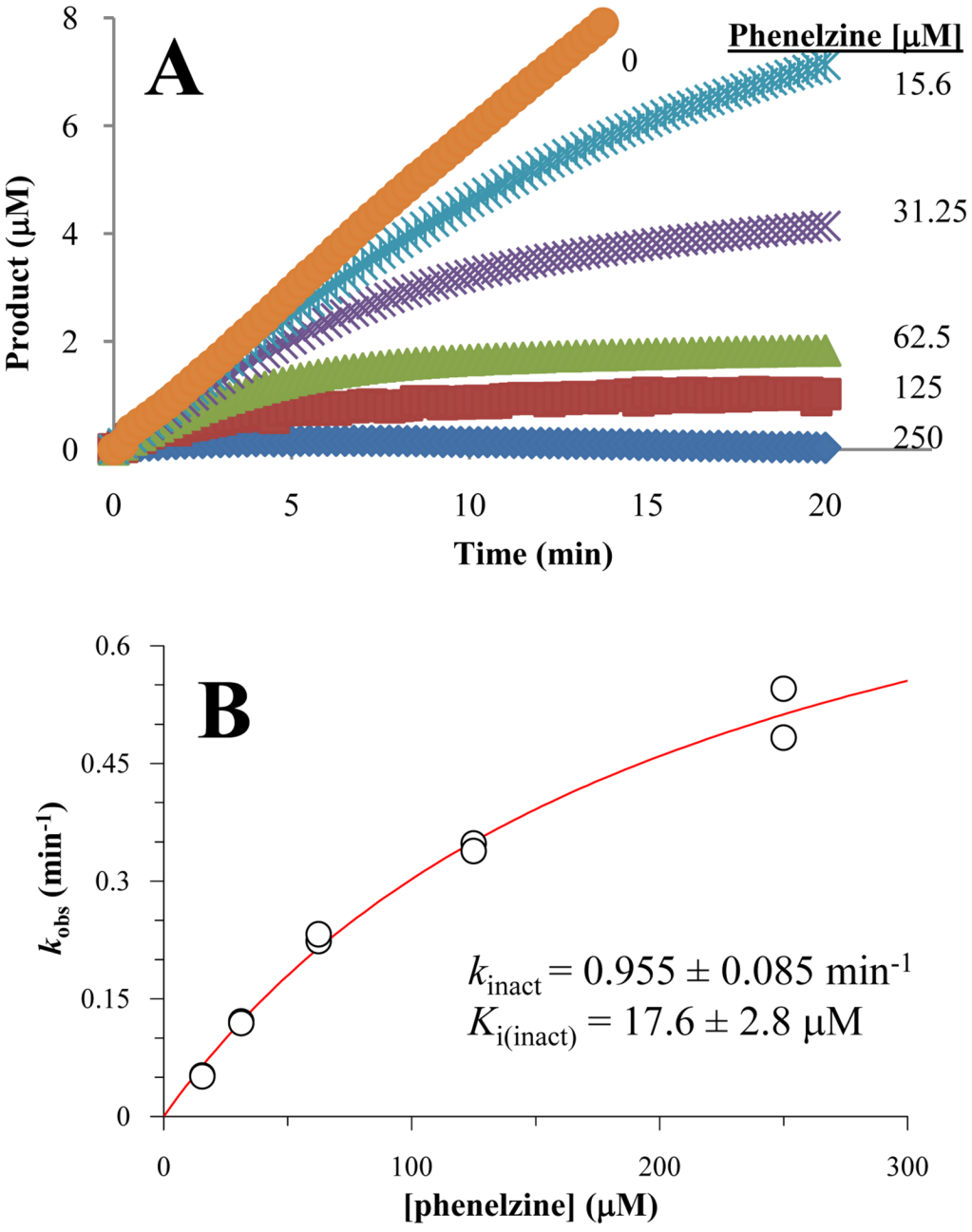

Figure 8.

Time- and concentration-dependent inactivation of GST-LSD1 by the small molecule MAO inactivator phenelzine. A) Steady-state progress curves obtained for the inactivation of LSD1 in the presence of concentrations of phenelzine ranging from 15.6 to 250 μM. B) Rate constants (k_{obs}) for the time-dependent inactivation of LSD1 by phenelzine were extracted from the steady-state data in A by single exponential fits and analyzed by the method of Kitz and Wilson to determine k_{inact} and $K_{i(inact)}$ values.

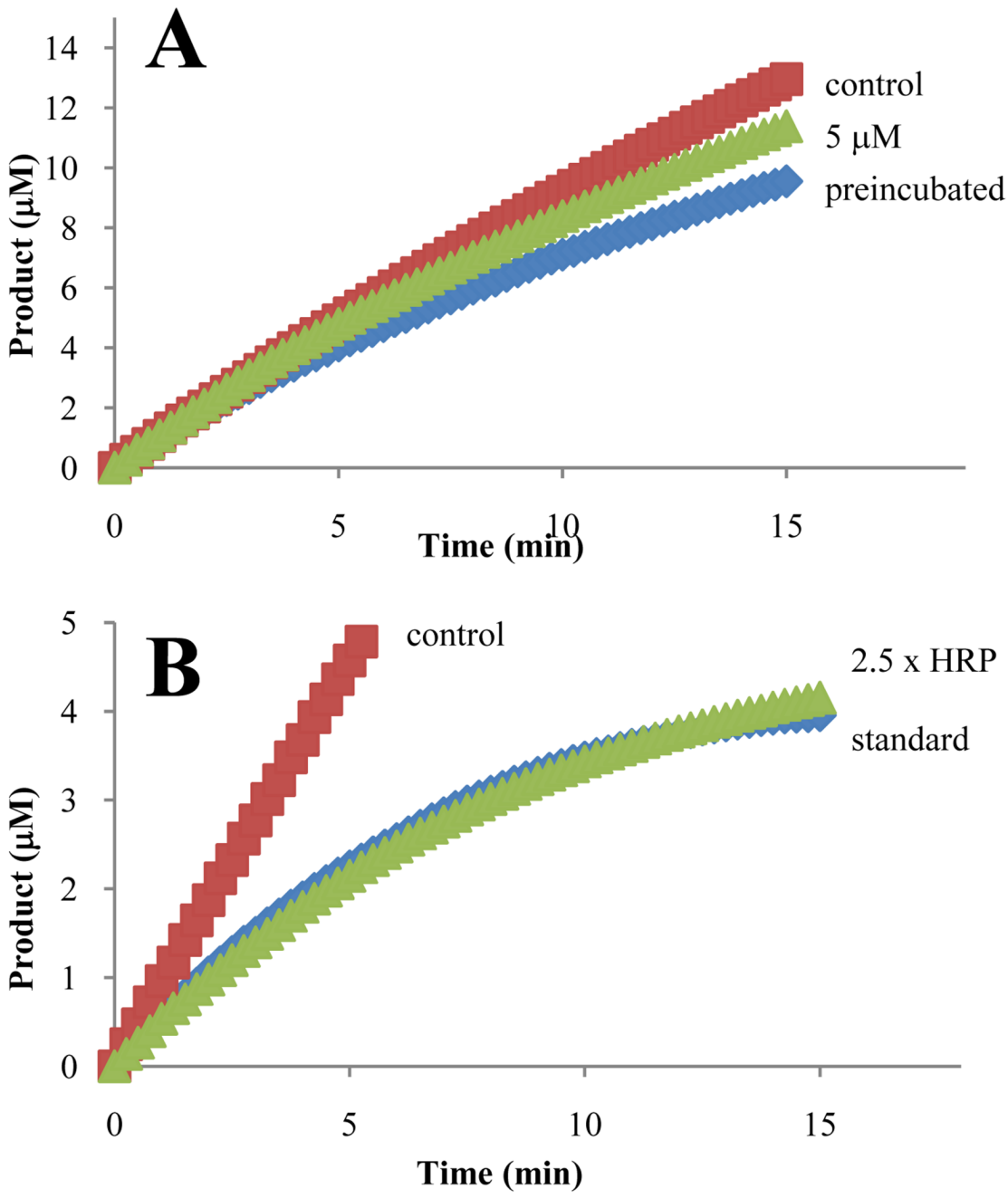

Figure 9.
GST-LSD1 inactivation by phenelzine. A) LSD1 inactivation is more pronounced when preincubated with phenelzine. B) LSD1 inactivation is independent of the horseradish peroxidase coenzyme concentration.

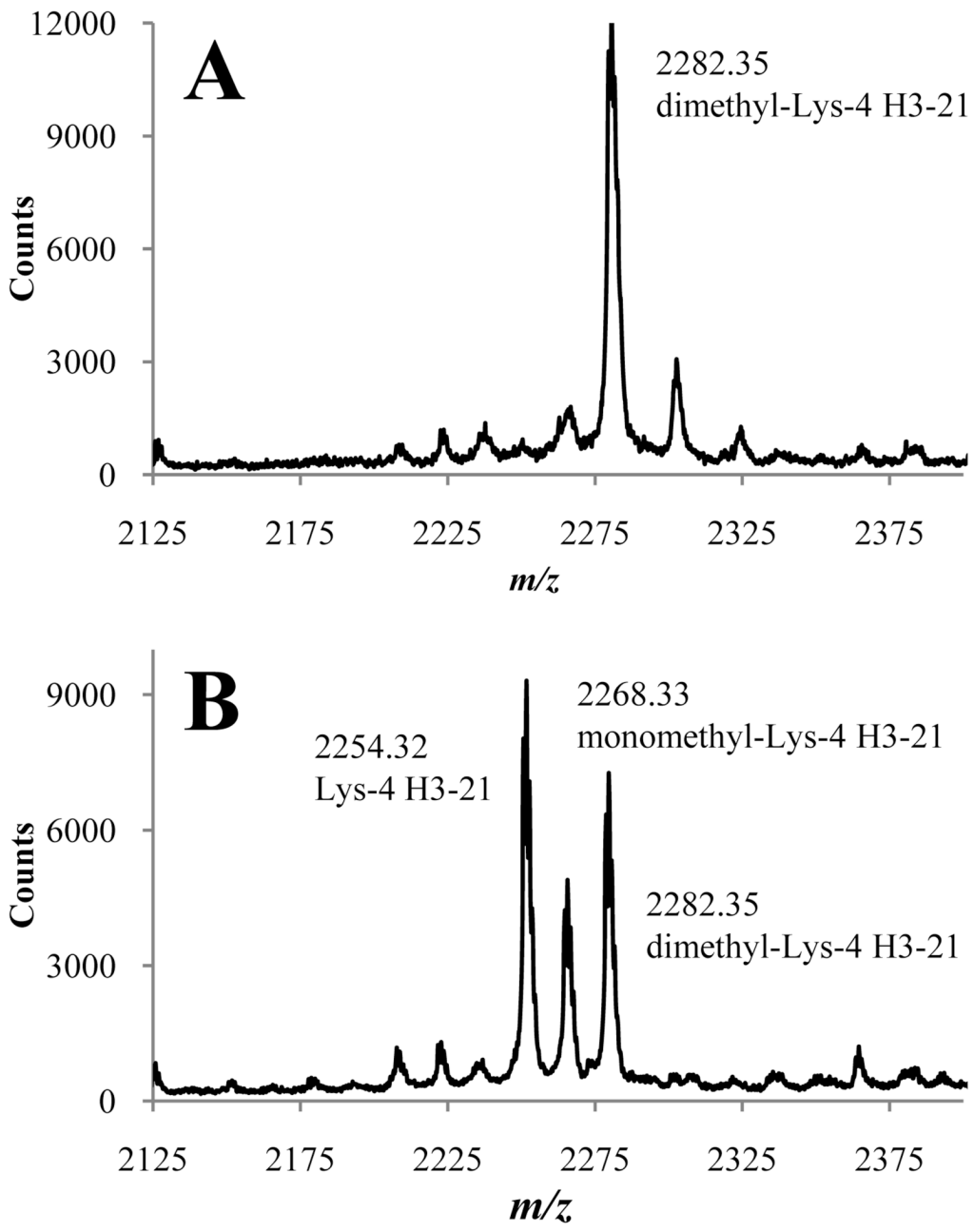

Figure 10.
MALDI-TOF assay demonstrating the inactivation of GST-LSD1 by phenelzine. A) LSD1 preincubated with phenelzine prior to exposure to dimethyl-Lys-4 H3-21 substrate fails to appreciably demethylate. B) LSD1 efficiently demethylates dimethyl-Lys-4 H3-21 substrate yielding monomethyl Lys-4 H3-21 and Lys-4 H3-21.

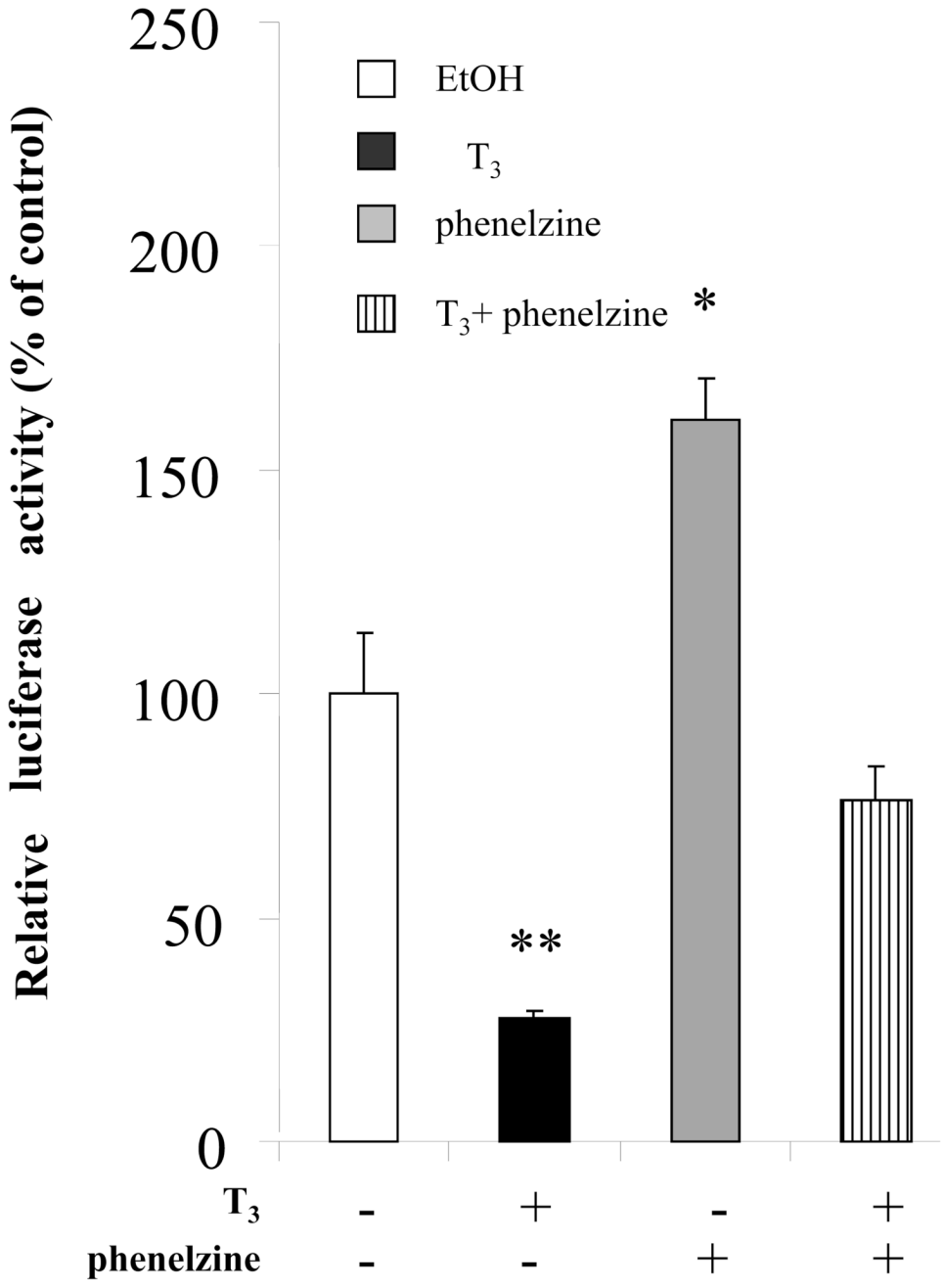

Figure 11.

T_3 and phenelzine effects on TSHα promoter activity and Lys-4 H3 methylation. α-23 cells were treated 24 hours with no hormone/phenelzine (control), 0.1 μM T_3, 10 μM phenelzine, or both. The cell lysates were prepared and luciferase activities were measured as described in Materials and Methods. Shown are the mean of triplicate samples ± SD. normalized to control as 100%. Similar findings were found in two other experiments. Data were analyzed by ANOVA and * = $p < 0.05$ and ** = $p < 0.01$ difference between indicated samples and EtOH control samples.

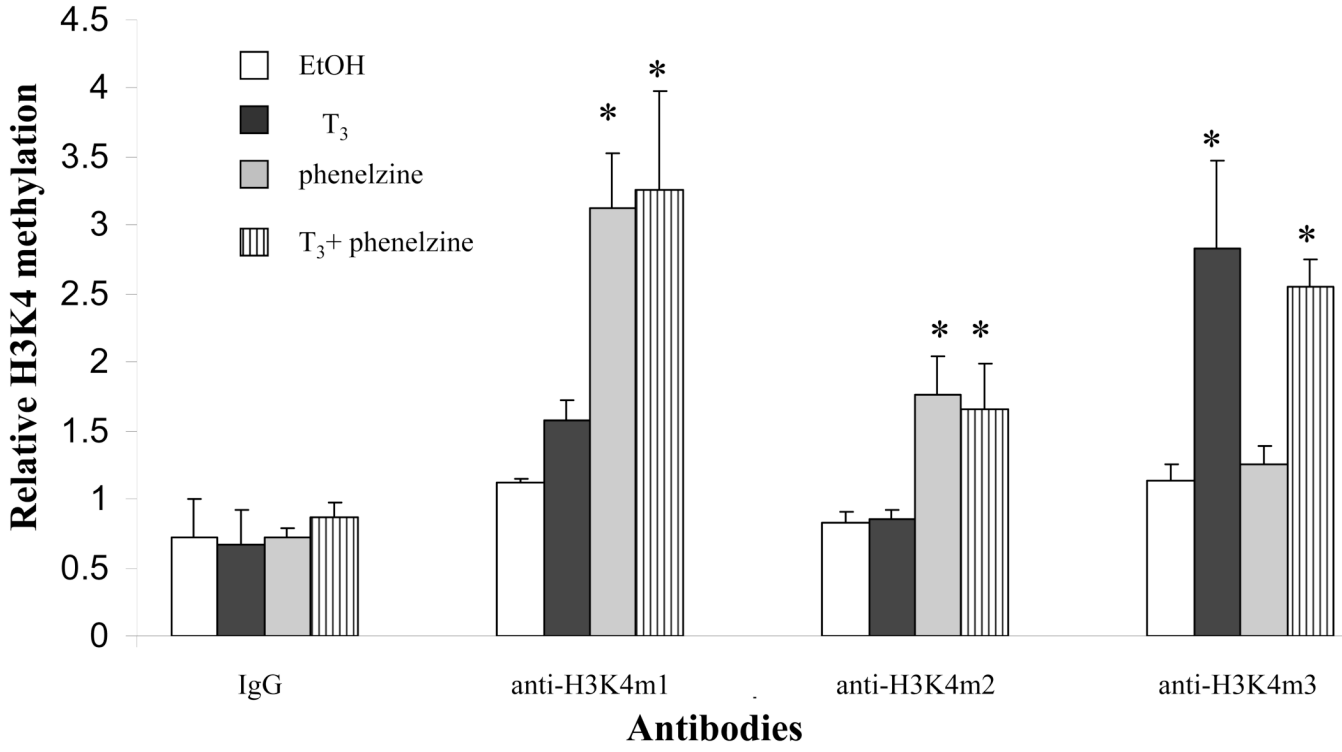

Figure 12.

T_3 and phenelzine regulation of methylation of Lys-4 H3. ChIP assay was performed as described in the Experimental section using antibodies against mono-, di- and tri-methylated H3K4. Similar findings were observed in two other experiments. Note: "-" indicates no hormone or phenelzine treatment. The Y axis shows relative H3K4 methylation based upon changes in cycle threshold number above background after each treatment. Data were analyzed by ANOVA and * = $p < 0.05$ difference between indicated samples and EtOH control samples.

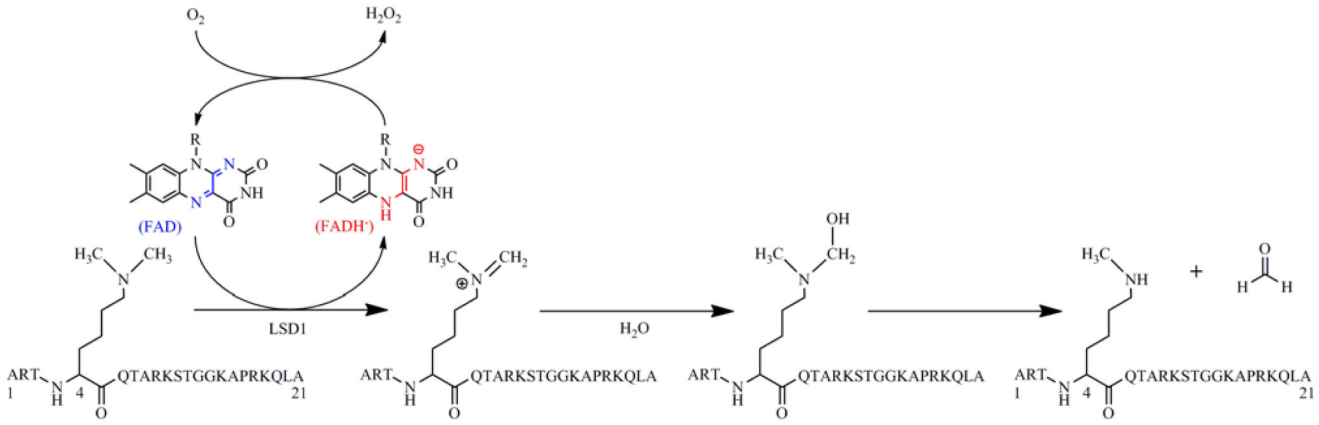

Scheme 1.

Catalytic cycle of flavin mediated amine oxidation. Oxidation of the amine to an iminium ion, with concurrent reduction of the flavin enables attack by a closely held water molecule. Collapse of the hemiaminal to a carbonyl yields formaldehyde and amine. Reduced flavin is re-oxidized by molecular oxygen, generating a molecule of hydrogen peroxide.

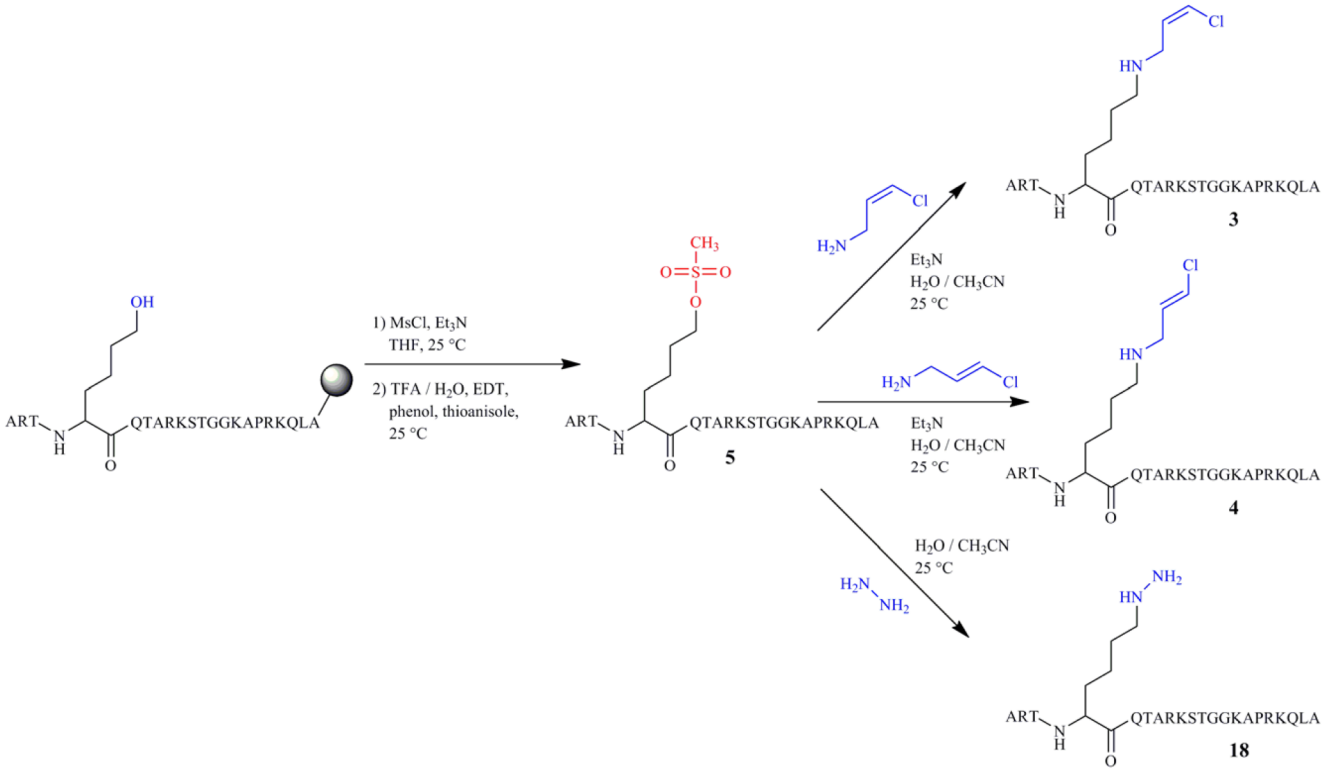

Scheme 2.

Synthesis of peptide inhibitors *cis*-3-chloroallyl-Lys-4 H3-21 (**3**), *trans*-3-chloroallyl-Lys-4 H3-21 (**4**) and hydrazino-Lys-4 H3-21 (**18**). Incorporation of Fmoc-hydroxynorleucine in the four position of H3-21 yields the resin bound peptide. Mesylation of the alcohol while on bead, followed by trifluoroacetic acid cleavage and RP-HPLC purification provides mesyl-Lys-4 H3-21 peptide **5**. Displacement of the mesylate by *cis* or *trans*-3-chloroallylamine or hydrazine yields the desired peptide inhibitors. Single letter amino acid abbreviations represent the H3-21 sequence.

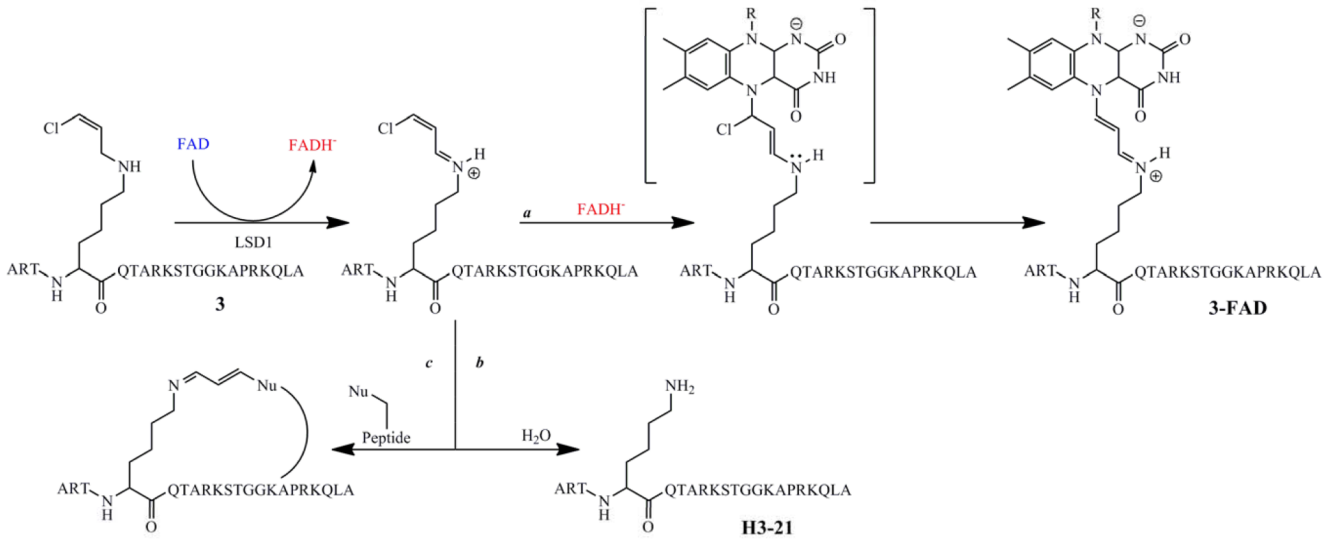

Scheme 3.

Proposed mechanism of inactivation of GST-LSD1 by *cis*-3-chloroallyl-Lys-4 H3-21 (**3**). Flavin mediated two electron oxidation of **3** yields an α,β-unsaturated iminium species. Pathway *a*) Nucleophilic attack by the N^5 of the reduced flavin leads to an α-chloro eneamine intermediate. Subsequent loss of the chloride atom forms the conjugated diamine linked **3**-FAD conjugate. Pathway *b*) Nucleophilic attack on the activated species by a water molecule leads to H3-21 peptide degradation product. Pathway *c*) Nucleophilic attack on the activated species by a nucleophile contained in the peptide leads to a cyclic peptide degradation product.

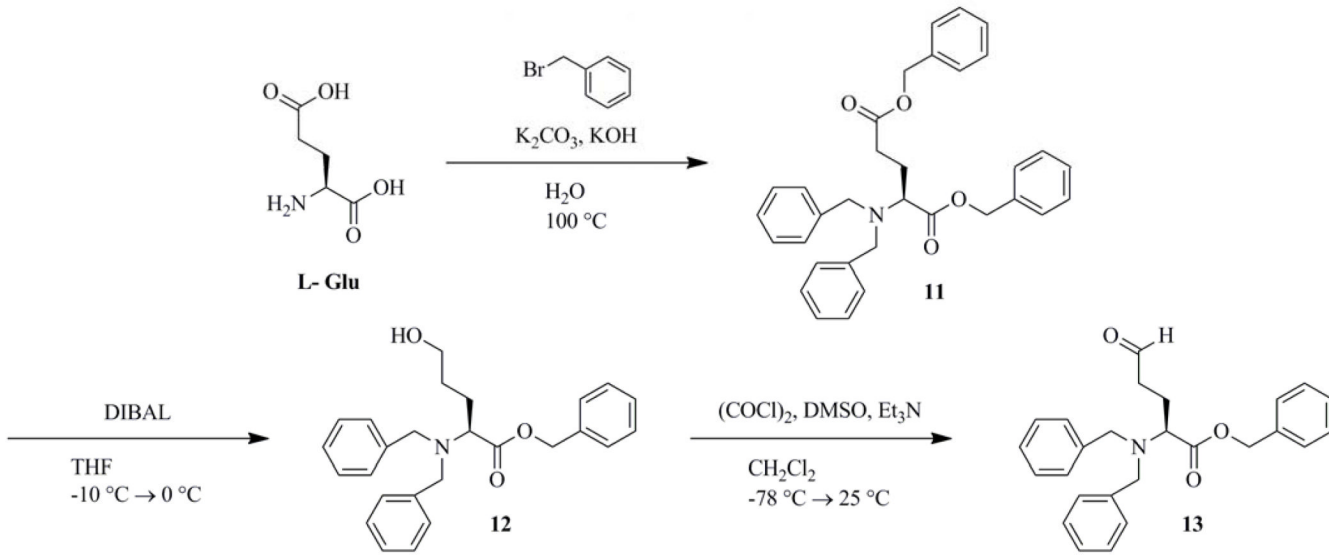

Scheme 4.
Synthesis of the amino aldehyde (S)-benzyl 2-(dibenzylamino)-5-oxopentanoate (**13**).

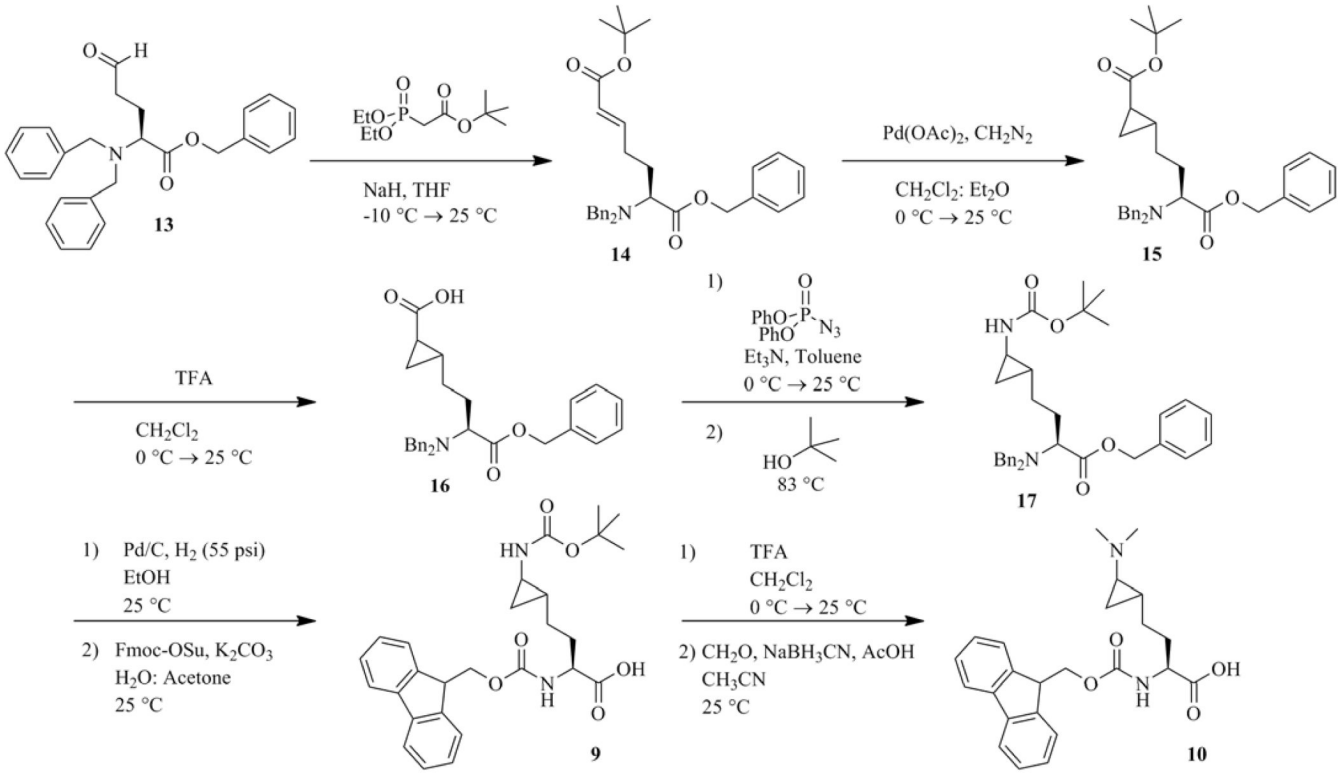

Scheme 5.

Synthesis of Fmoc-*endo*-cyclopropyl-Lys(Boc)-OH (**9**) and Fmoc-*endo*-dimethylcyclopropyl-Lys-OH (**10**).

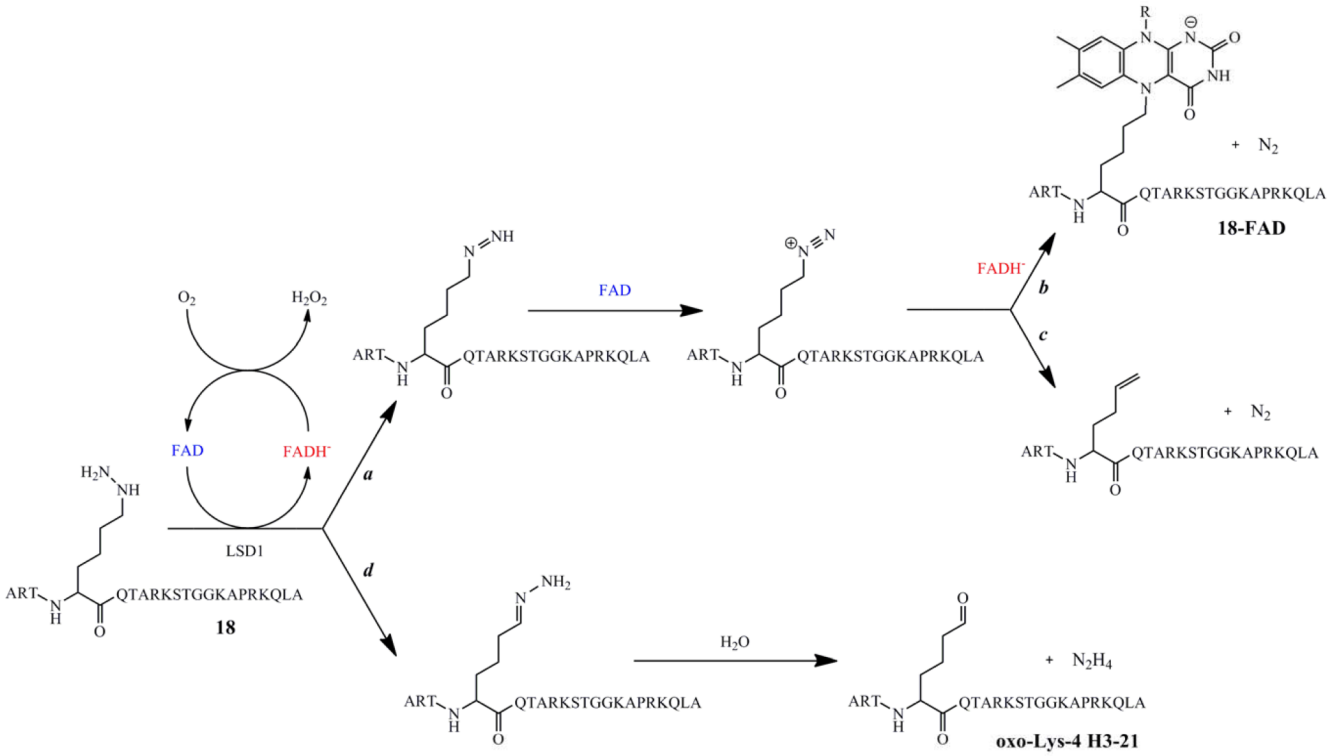

Scheme 6.

Proposed mechanism of inactivation of GST-LSD1 by hydrazino-Lys-4 H3-21 (**18**). Pathway *a*, two electron oxidation of **18** by the flavin yields the diazene. A second oxidation to the primary diazonium species produces a powerful electrophilic site at the alpha carbon. Pathway *b*, nucleophilic attack by the flavin N^5 yields inactivated LSD1 as an **18**-FAD adduct. Pathway *c*, abstraction of the beta proton leads to the olefin through lose of N_2. Pathway *d*, the competing oxidation leads to the formation of the hydrazone which can non-enzymatically hydrolyze to the aldehyde containing peptide oxo-Lys-4 H3-21.

Table 1

Kinetics of evaluated GST-LSD1 inhibitor and inactivator peptides and small molecules. Data for compounds **1**, **2**, **6**, and tranylcypromine has been obtained previously.[20–23]

Inhibitor / Inactivator	$K_{i(inact)}$ (μM)	$k_{(inact)}$ (min^{-1})	$k_{(inact)}/K_{i(inact)}$ ($\mu M^{-1}\ min^{-1}$)	K_i (μM)
propargyl-Lys-4 H3-21 (**1**)	0.775 ± 0.16	0.304 ± 0.033	0.392 ± 0.0088	-
N-methylpropargyl-Lys-4 H3-21 (**2**)	0.107 ± 0.057	0.208 ± 0.068	1.94 ± 0.34	-
cis-3-chloroallyl-Lys-4 H3-21 (**3**)	0.955 ± 0.15	0.545 ± 0.038	0.571 ± 0.0062	-
trans-3-chloroallyl-Lys-4 H3-21 (**4**)	0.763 ± 0.12	0.128 ± 0.0087	0.168 ± 0.0018	-
exo-cyclopropyl-Lys-4 H3-21 (**6**)	-	-	-	2.70 ± 0.74
endo-cyclopropyl-Lys-4 H3-21 (**7**)	-	-	-	6.11 ± 0.86
endo-dimethylcyclopropyl-Lys-4 H3-21 (**8**)	-	-	-	24.2 ± 2.7
hydrazino-Lys-4 H3-21 (**18**)	0.00435 ± 0.00086	0.247 ± 0.018	56.8 ± 0.82	-
tranylcypromine	357 ± 120	0.542 ± 0.094	0.00152 ± 0.000089	-
phenelzine	17.6 ± 2.8	0.955 ± 0.085	0.0543 ± 0.00077	-